December 2020

A Study of the Synthesis of Cellulose by the Bacteria *Komagataeibacter xylinus* (*K. xylinus*) when Under the Action of an Electric Field in a Microfluidic Reactor

Sindora Baddam
Clemson University, sbaddam@clemson.edu

A STUDY OF THE SYNTHESIS OF CELLULOSE BY THE BACTERIA *KOMAGATAEIBACTER XYLINUS* (*K. XYLINUS*) WHEN UNDER THE ACTION OF AN ELECTRIC FIELD IN A MICROFLUIDIC REACTOR

A Thesis
Presented to
the Graduate School of
Clemson University

In Partial Fulfillment
of the Requirements for the Degree
Master of Science
Mechanical Engineering

---

by
Sindora Reddy Baddam
December 2020

Accepted by:
Dr. Rodrigo Martinez-Duarte, Committee Chair
Dr. Xianchung Xuan
Dr. Phanindra Tallapragada

ABSTRACT

Dielectrophoresis (DEP) is an established technique used as a label-free method to manipulate microorganisms by exploiting the interaction of targeted microorganisms with a non-uniform electric field. The strength and direction of the DEP force on a targeted cell, specifically Komagataeibacter xylinus (*K. xylinus*), is dependent on the frequency of the applied electric field as well as the dielectric properties of the bacterial cell and suspending media.

K. xylinus is a microorganism that can synthesize a fibrous, web-shaped organic material called bacterial cellulose (BC), which contains desirable properties such as high mechanical strength and increased water holding capabilities. By combining DEP techniques with this BC synthesizing microorganism, this creates the potential for controlled and enhanced growth allowing BC to be tailored to specific properties at specific locations. However, literature has reported limited information regarding the use of DEP techniques to study how electric fields affect BC synthesis in a microfluidic reactor.

In this study, a titanium-based semicircular microelectrode chip was used to study how electrostimulation can potentially manipulate and influence the synthesis of BC at unique regions of interest where the electric field is greatest. This study features experiments running over fourteen days with an AC induced electric field at polarization voltages of 1 V_{pp}, 2 V_{pp}, and 5 V_{pp} at a frequency of 750 kHz. Results suggest that BC

synthesis is possible and can be manipulated over an extended period as the polarization voltage increased where the electric field is greatest.

DEDICATION

This thesis is dedicated to my family, friends, and mentors. I would like to give a special thanks to my parents Sabitha and Narender, and my sister Seema. Thank you all for the unconditional love and support all these years! I could not have done this without you guys!

ACKNOWLEDGMENTS

I would first like to thank my advisor Dr. Rodrigo Martinez-Duarte for his help and guidance throughout this project. I want to thank my undergraduate advisor Dr. Daniel Conway in the Biomedical Engineering Department at Virginia Commonwealth University (VCU) for his continuing advice and guidance throughout my academic and professional career over the years. I also want to thank the Mechanical Engineering Department at Clemson University, and all my fellow graduate students for all the love and support necessary to complete my thesis. I want to give an additional thanks to Dr. Mark Blenner and his research group in the Chemical Engineering Department for allowing me to use their resources and answer any questions for cell culture work. Finally, I want to personally thank Blake Betsill, Devin Keck, Tiffany Wong, Brittany Allen, Jewell Brey, Christina Ha, Caroline Buck, John Kremar, William McCormack, Matt Williams, Sara Damas, and Mavi Elena for various research endeavors. Thank you all!

TABLE OF CONTENTS

Page

TITLE PAGE i

ABSTRACT ii

DEDICATION iv

ACKNOWLEDGMENTS v

LIST OF TABLES ix

LIST OF FIGURES x

CHAPTER

I. Introduction 1

1.1 Motivation 1

II. State of the Art 4

2.1 Komagataeibacter xylinus (*K. xylinus*) – A Bacterial Cellulose Producing Microorganism 4

2.2 Bacterial Cellulose Synthesis 5

2.3 The Use of Electric Fields on Microorganisms 7

2.4 The Study and Effect of Dielectrophoretic Induced Electric Fields on Microorganisms for Biological Applications 10

2.5 The Study and Effect of Electric Fields on *K. xylinus* and Bacterial Cellulose Synthesis 13

2.6 Bacterial Cellulose Stains for Imaging – Direct Red 23 and Calcofluor White 17

III. Theoretical Background 19

3.1 Electrical Polarization 19

3.2 Dielectrophoresis (DEP) 19

3.2.1 DEP Force on A Particle 22

3.2.2 The Shell Model 22

3.3 Electroporation 24

3.4 Electrical Lysis 25

3.5 Electrochemical Stability of Titanium 26

IV. Materials and Methods 27

4.1 Culture of *K. xylinus* and Experimental Media 27

4.2 Computational Modeling of the Electric Field Around Microelectrodes 28

4.3 Device Fabrication 31

4.3.1 Titanium (Ti)-Microelectrode Devices 32

4.3.2 Indium Tin Oxide (ITO)-Microelectrode Devices 33

4.3.3 Finalized Device 34

4.4 Experimental Platform and Protocol to Characterize Frequency Response and Bacterial Cellulose Synthesis Under an Electric Field 36

4.4.1 Experimental Protocol – Frequency Characterization 37

4.4.2 Experimental Protocol – Bacterial Cellulose Synthesis 38

4.5 Data Acquisition 39

4.5.1 Frequency Characterization 39

4.5.2 Bacterial Cellulose Synthesis 40

V. Results and Discussion 42

5.1 Computational Modeling Results 42

5.2 Frequency Response of *K. xylinus* Based on Culture Age..... 44

5.3 Bacterial Cellulose Synthesis Under and Electric Field Results at 1 V_{pp}, 2 V_{pp}, and 5 V_{pp} 48

5.3.1 A Closer Look at 1 V_{pp} With Modified Results..... 56

5.3.1 Region 5 Results of Bacterial Cellulose Synthesis..... 57

5.4 Discussion..... 59

VI. Conclusions and Future Work 62

6.1 Conclusion 62

6.2 Future Work..... 62

REFERENCES 64

APPENDICES 69

A: Oxalic Acid Etch Rates for ITO-Microelectrode Devices 69

B: Fluorescent and Brightfield Plots for Region 4A and Region 5 71

LIST OF TABLES

Table Page

1 Review of Published Studies Using Electric Fields and Analyzing Its Effects on Microorganisms. 9

2 Review of Published Studies Using DEP Techniques to Induce Electric Fields and Analyzing Its Effects on Microorganisms..... 12

3 Review of Published Studies Using Electric Fields and Analyzing Its Effects on *K. xylinus* and its Effect on Bacterial Cellulose Synthesis 15

4 Variables for Equation 9 and 10 for Hydrophilic and Hydrophobic Pore Energy 25

5 Summary of the Fluorescent and Control Change in Intensity for Region 4A at Day 14 53

6 Summary of the Brightfield and Control Change in Intensity for Region 4A at Day 14 53

LIST OF FIGURES

Figure Page

1 *K. xylinus* and its sub-elementary nanofibrils forming a collection of microfibrils. A collection of microfibrils creates the bundles of cellulose for the web-shaped BC network 5

2 Bacterial cellulose grown in a macro environment and cleaned with 0.1 M NaOH 6

3 Brief explanation of the biosynthesis process and pathways for bacterial cellulose by *K. xylinus.* Glucose is phosphorylated by the UDP-glucose pyrophosphorylase. In the last enzymatic step, cellulose synthase synthesizes cellulose. The other metabolic pathways shown (TCA, ADP to ATP, etc.) provide necessary functional groups for synthesizing BC. BC is extruded out of the cell creating the bacterial cellulose network..... 7

4 Image of *K. xylinus* culture grown in 15 mL tubes. The top opaque layer indicates a healthy layer of BC forming on top 28

5 Semicircular microelectrode design chosen..... 29

6 Screenshot of the ANSYS workspace highlighting the boundary conditions and Ti-microelectrode design with specific set parameters..... 30

7 Unique regions of interest drawn for Region 1, 2, 3 4, 4A, 5, and 6 based on the ANSYS simulation results and using the center-to-center distance of the semicircle. This is to account for all potential bacterial cells trapped at the leading edges of the Ti-electrodes. Region 4A indicates the strongest electric field for studying BC synthesis 31

8 Ti-Microelectrode Device Fabrication Process 33

9 Indium Tin Oxide (ITO)-Microelectrode Device Fabrication Process 34

10 Finalized Chip..... 35

11 Top View of the Ti-microchip featuring 6 rows x 32 columns of semicircular microelectrodes. Each electrode is spaced 300 μm apart based on the center-to-center distance of the semicircle. The field of view features only

8 electrodes for analysis while taking live cell images under the microscope 36

12 Experimental Set-up Overview 37

13 Brightfield and Fluorescent image view under the microscope with regions of interest overtop for post-processing in ImageJ 39

14 Modeling of the Electric Field for the Ti-microelectrodes at different voltages. The modeled media around the electrodes was water with an electrical conductivity of 504 μS/cm. The simulations show that the magnitude of the electric field is directly proportional to voltage. By keeping the magnitude less than 10^5 V/m, this ensures optimal cell viability of *K. xylinus* and prevents electrical lysis. The simulations indicate that electrical lysis may start to occur at 7 V_{pp} as shown in the orange-red regions in the figure 43

15 Modeling of the distribution of the Electric Field Gradient in the microfluidic reactor when the Ti-microelectrodes are polarized at 1 V_{pp}, 2 V_{pp}, 5 V_{pp}, and 7 V_{pp}. The modeled media around the electrodes was water with an electrical conductivity of 504 μS/cm. When *K. xylinus* experiences a positive DEP force, they are expected to migrate towards the regions of the highest electric field gradient, as shown in the green-yellow colors in the figure 44

16 Raw Data for Average Percent Change in Intensity Over Time. This plot represents the trapping behavior of *K. xylinus* on the Ti-microelectrode over a 90 second time span. The plot indicates important areas such as the 0-10 second mark where the electric field is turned on and the 10-15 second mark where the electric field is tuned off. This 10-15 second mark is the data analysis region to monitor how the bacterial cells behave as it crosses over the data analysis region when the field it turned off as indicated by change in intensity. The last 40-90 seconds show a stagnant change in intensity
..... 46

17 24, 48, and 96 hour DEP response from 250 kHz to 10 MHz with 500 kHz generating the strongest DEP response and change in intensity 47

18 Complete Analysis of Experiment 1 at 5 V_{pp} for All Regions for the Fluorescent and Brightfield Change in Intensity 48

19 Plot of the Fluorescent Intensity versus Control Intensity and their standard deviations for Region 4A at 1 V_{pp}. This data represents the average of 8

Ti-microelectrodes per experiment (24 Ti-microelectrodes total) for the Fluorescent data and the Control data.....50

20 Plot of the Brightfield Intensity versus Control Intensity and their standard deviations for Region 4A at 1 Vpp. This data represents the average of 8 Ti-microelectrodes per experiment (24 Ti-microelectrodes total) for the Brightfield data and the Control data.....50

21 Plot of the Fluorescent Intensity versus Control Intensity and their standard deviations for Region 4A at 2 V_{pp}. This data represents the average of 8 Ti-microelectrodes per experiment (24 Ti-microelectrodes total) for the Fluorescent data and the Control data.....51

22 Plot of the Brightfield Intensity versus Control Intensity and their standard deviations for Region 4A at 2 V_{pp}. This data represents the average of 8 Ti-microelectrodes per experiment (24 Ti-microelectrodes total) for the Brightfield data and the Control data.....51

23 Plot of the Fluorescent Intensity versus Control Intensity and their standard deviations for Region 4A at 5 V_{pp}. This data represents the average of 8 Ti-microelectrodes per experiment (24 Ti-microelectrodes total) for the Fluorescent data and the Control data.....52

24 Plot of the Brightfield Intensity versus Control Intensity and their standard deviations for Region 4A at 5 V_{pp}. This data represents the average of 8 Ti-microelectrodes per experiment (24 Ti-microelectrodes total) for the Brightfield data and the Control data.....52

25 Plot of the Fluorescent Intensity for Region 4A at all voltages (1 V_{pp}, 2 V_{pp}, and 5 V_{pp}). This data represents the difference of the Fluorescent data and the Control data to normalize the results. It can be seen that 5 V_{pp} shows the greatest Change in Intensity and 1 V_{pp} with the least Change in Intensity.....54

26 Plot of the Brightfield Intensity for Region 4A at all voltages (1 V_{pp}, 2 V_{pp}, and 5 V_{pp}). This data represents the difference of the Brightfield data and the Control data to normalize the results. It can be seen that the intensity slightly trends upward with the exception of 2 V_{pp} 55

27 Plot of the Fluorescent Intensity versus Control Intensity and their standard deviations for Region 4A at 5 V_{pp} and then changed to 1 V_{pp} after the bacterial cells stabilized. This data represents the average of 8 Ti-microelectrodes per experiment (24 Ti-microelectrodes total) for the Fluorescent data and the Control data.....56

28 Cross-sectional Modeling of the Electric Field for the 350 nm high Ti-microelectrodes at 5 V_{pp} to further analyze Region 5. The modeled media around the electrodes was water with an electrical conductivity of 504 µS/cm. The simulations show that the magnitude of the electric field is directly. By keeping the magnitude less than 10^5 V/m, this ensures optimal cell viability of *K. xylinus* and prevents electrical lysis.....57

29 Plot of the Fluorescent Intensity for Region 5 at all voltages (1 V_{pp}, 2 V_{pp}, and 5 V_{pp}). This data represents the difference of the Fluorescent data and the Control data to normalize the results. It can be seen that 5 V_{pp} shows the greatest Change in Intensity and 1 V_{pp} with the least Change in Intensity 58

CHAPTER ONE

INTRODUCTION

1.1 Motivation

Cellulose is an organic compound, a polysaccharide, which plays an integral role in the structural component in cell walls of plants. It is made of linear polymer chains of b-1,4-linked glucose residues [12]. Cellulose can be found in materials such as cotton, wood, hemp, paper, and synthesized by bacteria. This compound is arranged in microfibril bundles giving it a desirable high strength and unique mechanical properties. Depending on where the source of cellulose is obtained, the physical properties of its crystalline state is highly variable [12].

Certain types of bacteria are able to naturally synthesize a form of cellulose giving it unique properties. Unlike plant cells, bacterial cellulose (BC) is a pure form of cellulose free of lignans and hemicellulose, which are typically found in plants [8]. Unlike cellulose synthesized by plants, bacterial microfibrils are 100-fold smaller. Compared to traditional sources of nanocellulose from plants sources, BC provides a pure form of cellulose with its higher crystallinity, a smaller crystallite size, and a higher elastic modulus and tensile strength [1, 12, 18]. Our research group focuses on studying the synthesis of BC for new applications.

BC is an organic material synthesized by certain types of bacteria, specifically, Komagataeibacter xylinus (*K. xylinus*). Materials such as BC can be found in nature and have desirable properties due to fibril bundles providing advantages such as high mechanical strength and increased water holding ability [1]. *K. xylinus* can synthesize BC in various environments allowing for controlled and enhanced growth, allowing the cellulose to be tailored to specific properties. Using *K. xylinus* to synthesize BC has numerous applications in biotechnology, materials science, and commercial applications [23].

The long-term goal of our research group is to use individual living microbes as "robotic print heads" to deposit nanomaterials at specific locations. By doing so, we can orchestrate the movement of living microbes using a nano-printing platform where nanolattices can be built in desired locations, tailoring it to specific material properties. While there has been considerable research focused on a range of methods for manufacturing of nanolattices, the use of individual microbes as robotic printing heads is not reported in literature, which can make advances in nano-scale additive manufacturing. Many of these microorganisms secrete nanomaterials with characteristic dimensions less that few tens of nanometers unlike traditional additive manufacturing techniques limited to the microscale [4, 18].

The research goal of this project is to study and understand the frequency response of *K. xylinus* and its cellulose synthesis production while under an electric field. By doing so, this would provide the potential to manipulate cellulose synthesis to arbitrary locations using a technique called dielectrophoresis (DEP). This allows us to use

DEP as a label-free technique to achieve spatiotemporal manipulation of *K. xylinus* to manipulate BC synthesis at desired locations to specific material properties.

Literature has reported that bacterial cells can be manipulated using DEP and has the potential to synthesize cellulose on a micro and macro scale while under an electric field. However, it is unknown how *K. xylinus* and bacterial cellulose behaves while using different magnitudes of electric fields in a microfluidic reactor. Limited knowledge has been reported regarding the use of DEP to analyze BC synthesizing microorganisms and their response to varying magnitudes of electric field, which is especially true in a microfluidic reactor. I believe that we can use electrostimulation to manipulate and potentially influence the synthesis of bacterial cellulose. By doing so, we expect to manipulate these microorganisms to increase fabrication throughput and enable deposition of natural nanomaterials.

CHAPTER TWO

STATE OF THE ART

2.1 Komagataeibacter xylinus (*K. xylinus*) – A Bacterial Cellulose Producing Microorganism

K. xylinus, is a species that can efficiently synthesize cellulose among bacteria. This microorganism is widely researched in various published studies for its unique characteristics and its cellulose synthesizing capabilities. Among the types of bacteria that synthesize cellulose, *K. xylinus* is the most effective species for cellulose production [18]. This GRAM negative aerobic bacterium typically measures 0.5 – 0.8 μm and can secrete a collection of fibrils on a nanoscale around 100 nm and 100 μm in diameter and length, respectively with each individual fiber ranging from 2 – 4 nm in diameter [4, 18]. However, the collection of fibrils length and diameter can vary depending on the size of the culture. *K. xylinus* can grow simultaneously and synthesize BC at the same time giving the ability to maximize BC throughput. The BC wraps the bacteria making it difficult to release the cells from the BC network. Figure 1 provides an image of *K. xylinus* and its components to produce cellulose fibrils.

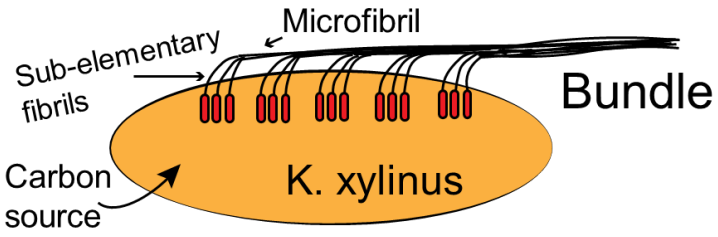

Figure 1: *K. xylinus* and its sub-elementary nanofibrils forming a collection of microfibrils. A collection of microfibrils creates the bundles of cellulose for the web-shaped BC network.

During the synthesis process, glucose chains are produced inside the bacterial body and then extruded via tiny pores in their cellular envelope [7]. This allows the glucose chains to form a network of ribbons made of cellulose, which create a collection of fibrils [7]. These fibril bundles together create a porous web-shaped matrix of BC.

2.2 Bacterial Cellulose Synthesis

How BC is synthesized under normal conditions by *K. xylinus* is critical on a biological level to study and understand the potential of electric fields on this microorganism. Under normal conditions, cellulose produced extracellularly is done at temperatures between 20 – 30 °C at a pH of 3 – 7 using glucose, fructose, sucrose, mannitol, and other carbohydrates [18]. Figure 2 represents what BC looks to the human eye after *K. xylinus* synthesizes cellulose and is cleaned with 0.1 M NaOH on a macro scale.

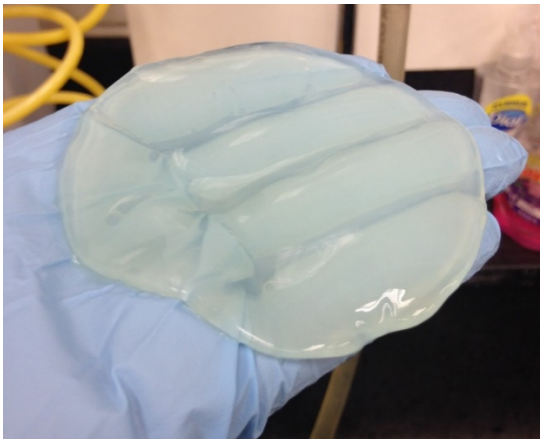

Figure 2: Bacterial Cellulose grown in a macro environment and cleaned with 0.1 M NaOH.

As briefly mentioned, BC is synthesized along the cell membrane. A protein in the membrane called the cellulose synthase complex polymerizes glucose to give rise to rigid chains of crystalline fibrils as it is extruded to the outer surface of the cell [2]. A basic fibril structure consists of a β−1→4 glucan chain, which is held together with hydrogen bonds with the following molecular formula: $(C_6H_{10}O_5)_n$ [7]. As more of these individual fibers bundle together, these glucose chains create the network and structure of BC in the form of a hydrogel sheet with high surface area and porosity giving rise to its unique characteristics of hydrophilicity, biodegradability, and chemical-modifying capacity [1, 3, 22, 23]. This multi-stop process involves a number of enzymes, and catalytic and regulatory proteins.

While there is a great amount of detail that goes into what these enzymes are and what is required for the regulatory pathways, a simplified explanation will be provided for understanding the context of this thesis. An overview can be seen in Figure 3. As mentioned, glucose is required to start the process, which is categorized into various enzymatic steps [33]. The final step for completing the phosphorylation of glucose is

completed by the enzyme, UDP-glucose pyrophosphorylase, followed by the synthesis of cellulose from cellulose synthase [33]. The rest of the metabolic pathways are completed by the Krebs cycle (TCA cycle), Adenosine di-phosphate (ADP) to Adenosine triphosphate (ATP) conversion, intake of fructose, intake of oxygen, and release of water. All of which, provide fundamental bonds and functional groups for synthesizing BC.

A general overview is shown in Figure 3 with important regulatory processes highlighted for *K. xylinus* synthesizing BC.

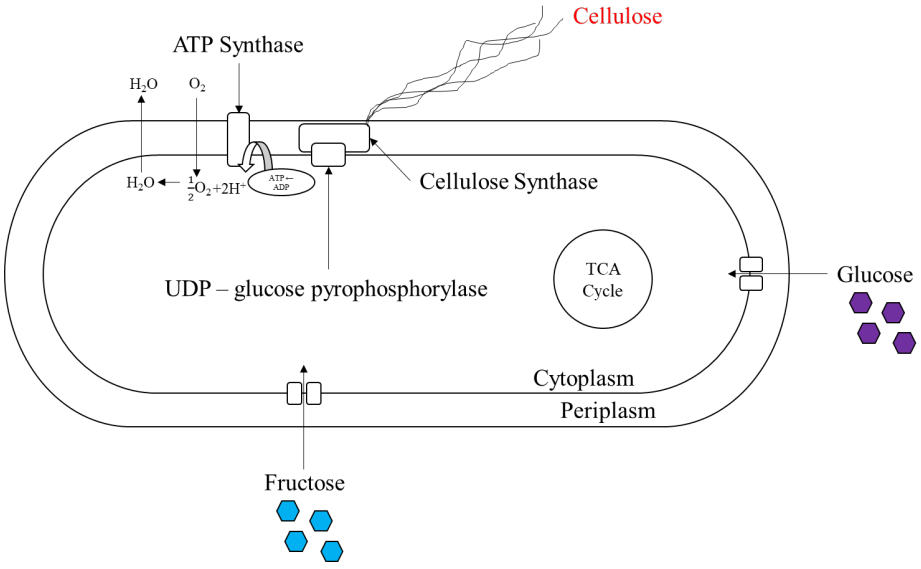

Figure 3: Brief explanation of the biosynthesis process and pathways for BC by *K. xylinus.* Glucose is phosphorylated by the UDP-glucose pyrophosphorylase. In the last enzymatic step, cellulose synthase synthesizes cellulose. The other metabolic pathways shown (TCA, ADP to ATP, etc.) provide necessary functional groups for synthesizing BC. BC is extruded out of the cell creating the BC network.

2.3 The Use of Electric Fields on Microorganisms

A few research groups have done some preliminary published work to introduce the use of electric fields on microorganisms such as bacterial and yeast cells. To fully understand the potential use of electric fields on *K. xylinus* for cellulose synthesis, it is

critical to understand what parameters researchers analyze to see how an electric field effects a microorganism.

Many early published studies highlight using electrostimulation by using pulsated electric fields (PEFs) to look at parameters such as electric field strength, the time duration while exposed to an electric field, the number of pulses for PEFs, temperature, pH, cell culture variations, and additional factors [35, 17]. Many of these parameters have shown varying affects depending on the microorganism when exposed to an electric field.

Table 1 below organizes a couple of published works studying the effect of electric fields and their effect on specific strains of microorganisms within yeast and bacteria cells. As mentioned, many of these initial studies feature PEFs. The goal is to see how an electric field can generally affect a microorganisms' response in general to further understand the potential of electric fields for cellulose synthesis production.

Organism(s)	Goal	Electric Field Parameters	Highlights on Main Findings	Reference
GRAM negative bacteria • Escherichia coli (*E. Coli*) • Klebsiella pneumoniae (*K. pneumoniae*) • Pseudomonas aeruginosa (*P. aeruginosa*) GRAM positive bacteria • Staphylococcus aureus (*S. Aureus*) • Listeria monocytogenes (*L. Monocytogenes*) Yeast Cells • Candida albicans (*C. albicans*)	Investigating the effects of electric fields on bacteria and yeast cells	PEFs with an electric field strength varied in steps of 2 kV/cm with pulse numbers of 2-30. An electrode area of 8.3 cm^2 with a distance of 0.5 cm was used.	GRAM positive bacteria and yeast cells were less sensitive to PEFs suggesting higher mechanical stability in their cell wall than GRAM negative bacteria. High PEFs suggest that their chance of survivability is low. Variations in microorganisms are due to changes in electric field strength, time exposure to electric fields, number of pulses, and cell viability. *E. Coli* with 4 hour versus 30 hours incubation have lower PEFs in 4 hours of incubation despite the pulse duration suggesting that PEFs vary biological physiology.	17
Bacteria Cells • Escherichia eoli (*E. Coli*) • Staphylococcus aureus (*S. Aureus*) • Miorococcus lysodeiktieus (*M. lysodeiktieus*) • Sarcina lutea (*S. Lutea*) • Bacillus subtilis (*B. Subtilis*) • Bacillus cereus (*B. cereus*) • Bacillus megaterium (*B. megaterium*) • Clostridium welchii (*C. welchii*) Yeast Cells • Saecharomyces Cerevisiae (*S. Cerevisiae*) • Candida utilis (*C. Utilis*)	Investigating the lethal effects of high electric fields (PEFs) on bacterial cells and yeast cells.	Rectangular DC pulses up to 10 kV with the pulse length varying from 2 - 20 µs in steps of 2 µs. Carbon electrodes with the field strength of less than 30 kV/cm.	Varying parameters of the lethal effects of DC pulses and the time of treatments varies between the microorganisms. The effect of altering pulse length was when shortened, more pulses were necessary for the same degree of cell death. When coming the pulse length and number of pulses, the results show the total time for which the voltage is applied is proportional. There was an insignificance in the electrolysis and heating of the samples.	35

Table 1: Review of Published Studies Using Electric Fields and Analyzing Its Effects on Microorganisms. This Table summarizes findings in literature and highlights parameters of interest regarding the use of electric fields on microorganisms such as yeast and bacteria.

Some notable findings feature variations in GRAM negative bacteria, GRAM positive bacteria, and yeast cells. While the goals of their studies are similar, their findings suggest that there are variations between a microorganisms' response to an electric field. For example, variations in electric field parameters such as strength and shape of the electric field, pulse duration, number of pulses, type of electrodes, time exposure to electric fields, etc. all affect the cell's response and survivability, which are

more prevalent in in GRAM positive and yeast cells. However, when all microorganisms are subjected to high PEFs, their chance of survivability is low. Other findings suggest that GRAM negative bacterial cells are more susceptible to morphological and structural changes in the cell wall and need further research, while others suggest that GRAM positive and yeast microorganisms have a higher mechanical stability in their cell wall and are less sensitive to PEFs. This allows us to think that by localizing the effect of electric fields to the cell wall, many papers start looking at how electric fields start generating a transmembrane potential since the integrity of the cell is sustained by the cell wall [34]. Due to this, studies have also shown that by varying cell incubation time (i.e. 24 hours, 48 hours, etc.) there are variations in the microorganism's response to an electric field despite the same electrical parameters suggesting that these changes could be due to the biological physiology of a cell. Changes in temperature and electrolysis have shown no significance in cell survivability, but changes in pH can create an inhabitable environment for microorganisms. This is due to the electrolysis of water dropping the pH of the medium the microorganisms are suspended in [19].

The main takeaway from these early studies suggests that electric fields affect biological processes in microorganisms, but many of these biological changes induced by an electric field are unknown and vary depending on the type of organism.

2.4 The Study and Effect of DEP Induced Electric Fields on Microorganisms for Biological Applications

As work in this field progresses, there are some limitations that need to better be understood on a biological level depending on the microorganism. Therefore, further studies have been published to understand how electric fields affect specific biological processes such as ion transport, physiological and polarity changes of intracellular components, and growth/metabolic processes. Many of these biological processes have been researched and analyzed using DEP techniques in microfluidic reactors. DEP techniques enable a frequency-selective method, which provides a label-free method to move and capture microorganisms, to induce an electric field based on the microorganism's characteristics (i.e. size, shape, intracellular components) without adverse effects in cell viability, damage to the cell wall, etc.

Table 2 below targets published studies done on electric fields and their effect on microorganisms by studying how DEP techniques in microfluidics are used to induce an electric field, which can affect biological processes. The goal is to see how dielectrophoretic techniques can directly affect a microorganisms' biological process to further understand the potential of electric fields for bacterial cellulose production.

Organism(s)	Goal	Electric Field Parameters	Highlights on Main Findings	Reference
Listeria monocytogenes (*L. monocytogenes*)	Investigating the effects of DEP on growth, viability, and immuno-reactivity of Listeria monocytogenes	Array of 40 interdigitated plantinum microelectrodes that is 25 µm wide spaced 25 µm apart on a flat silicon substrate and a chamber (50 µL capacity). • Negative DEP at 1 kHz and 3 Vpp • Both negative and positive DEP at 10 kHz and 3 Vpp • Positive DEP at 50 kHz and 3 Vpp	• 1 hour of DEP treatment increased the cell immuno-reactivity of the cell specific polyclonal antibodies by ~31.8% and the C11E9 monoclonal antibodies by ~82.9% • 1 hour of DEP treatment did not cause any change in the growth of cells in the low conductive growth medium. • 4 hours or greater of DEP treatment (5 MHz, 20 Vpp) reduced the viable cell numbers by 56.8–89.7 %. The results indicated that DEP manipulation may or may not affect the final detection signal in immuno-based detection depending on the type of antigen-antibody reaction involved. However, prolonged DEP treatment for manipulating bacterial cells could produce negative effects on the cell detection by growth-based methods.	36
• Saccharomyces cerevisiae (*S. cerevisiae*) • Saccharomycopsis lipolytica (*S. lipolytica*) • Schizosaccharomyces pombe (*S. pombe*) • Verticillium chlamydosporium (*V. chlamydosporium*) • Phycomyces blakesleeanus (*P. blakesleeanus*) • Penicillium expansum (*P. expansum*)	Investigating the DEP behavior of yeast cells and its effect on growth sources and the cell wall compared to fungal spores	RMS voltage of 40 V Conductivity of $2*10^{-3}$ S/m Frequency of 1 MHz.	Produced a dielectrophortic response that decreased based on the amount of sugar present. Growth of nonfermentable carbon sources produced a constant dielectrophoretic yield, except for *S. cerevisiae*, which was decreased. Meaning that the size of the particle is the main parameter that affects dielectrophoretic yield. The contribution of biological parameters, such as the metabolic state of the cells, the effect of the cell wall, growth sources, etc., must be evaluated for each species.	37

Table 2: Review of Published Studies Using DEP Techniques to Induce Electric Fields and Analyzing Its Effects on Microorganisms. This Table summarizes findings in literature and highlights parameters of interest regarding the use of DEP induced electric fields on microorganisms such as yeast and bacteria.

Based on the results of the table, even with DEP techniques, a microorganism's biological response to electric fields vary significantly. However, several published sources are able to show that GRAM positive, GRAM negative cells, and yeast cells vary due to variations in the cell wall components [34, 35, 37, 38]. This is because their cell wall is composed of polysaccharides and glycoproteins [38]. The cell membrane is composed of the lipid bilayer, giving each unique microorganism a unique electrical physiology, which arises from the organism itself, medium the cells are suspended in, and

functional groups necessary to form bonds [38]. A microorganism with the absence of the of the outer lipid membrane layer causes GRAM positive bacteria to have higher electrical conductivity than those of GRAM negative bacteria [38]. By having these unique characteristics and variations, this allows for selective polarization at different frequencies in DEP methods.

2.5 The Study and Effect of Electric Fields on *K. xylinus* and Bacterial Cellulose Synthesis

Having looked at initial studies of electric fields on various microorganisms and narrowing it down to how DEP techniques can affect a microorganisms' biological processes, now all of these components can be analyzed for *K. xylinus* as a BC producing organism. As for *K. xylinus* specifically, there is limited published work on electric fields and its effect on cellulose synthesis. This is especially true for using DEP techniques to induce electric fields. Few published works indicate that it is possible for BC to be synthesized while under an electric field in a micro and macro setting. However, little has been published regarding how different magnitudes of AC induced electric fields while using DEP directly affect cellulose synthesis in a microfluidic reactor. Also, there have been limited studies reported how electric fields affect *K. xylinus* on a biological level. The previous Table 1 and 2 were used to narrow down on how electric field parameters and DEP can be combined to analyze the BC synthesis process.

Table 3 below summarizes my literature review into certain parameters to further discuss findings in literature. Many papers of interest were targeting the bacterium *K.*

xylinus, but also feature other microorganisms and similar species within the group *xylinum* (BC producing species). This table summarizes unique characteristics and findings.

Organism(s)	Goal	Electric Field Parameters	Highlights on Main Findings	Reference
Gluconacetobacter xylinus (*G. xylinus*)	Investing metabolic process for synthesizing BC	DC electric fields at 10 mA with 2 Platinum electrodes with a diameter of 2 mm spaced 115 mm apart. Magnitude of 50 V/m.	BC synthesis at the cathode is promoted within 12 hours and BC synthesis and the anode was inhibited at 6 hours. These changes are due to effects of glycolysis, tricarboxylic acid cycle, and the presence of oxygen during the lactic acid cycle.	19
Gluconacetobacter xylinus (*G. xylinus*)	Investigating biochemical and cellular properties when exposed to Rotating magnetic fields (RMF)	RMF assisted bioreactor (f = 50 Hz, Magnetic field B = 34 mT, 28°C incubation temperature)	RMF intensified BC production and the biochemical process, and growth of the bacterium after 144 hours (72 hours incubation, and then 72 hours under RMF).This affects glucose consumption, concentration of acetic acid, and gluconic acid which influences the rate of cell metabolism.	24
Gluconacetobacter xylinus (*G. xylinus*)	Investigating electric fields to orient BC-glass fiber nanocomposites	DC electric fields at 10 mA. Magnitude of 40 kV/m.	A method has been developed to orient the nanofibers in the direction of the DC electric field to provide higher tensile properties and thermostability.	25
Gluconacetobacter xylinus (*G. xylinus*)	Investigating the feasibility of using irreversible electroporation to introduce pores in BC scaffolds	Electroporation using PEFs using stainless steel electrodes 300 µm apart and 1 mm apart at varying magnitudes of 12.5-17.5 kV/cm every 15-60 mins for 90 pulses	By using controlled irreversible electroporation, it prevented cellulose deposition in a particular area, thus lysing bacteria. By varying parameters such as voltage, number of pulses, frequency, and duration between treatments, they can create a localized pore in the scaffold.	26
Acetobacter xylinum (*A. xylinum*)	Investigate assembly of BC nanofibers	• 1 V, 2.5 V, 5 V, DC electric fields in a 1 cm long, 300 µm wide, 50 µm deep microfluidic channel using Aluminum microelectrodes • 10 V DC electric fields in a 100 mL beaker with Aluminum electrodes	*A. xylinum* can assemble BC from the bottom-up in micro- and macro-environments suggesting 3D bottom-up BC synthesis	9
Gluconacetobacter xylinus (*G. xylinus*)	Investigate the yield of BC and its material properties when exposed to different parameters of RMFs	RMF assisted bioreactor (f = 50 Hz, Magnetic field B = 34 mT, 28°C incubation temperature)	*G. xylinus* cultures exposed to the RMF for 72 hours incubation, and then 72 hours under RMF synthesized BC more than bacteria continuously exposed to RMF for 144 hours. This did not negatively affect the polymer material properties.	27
Acetobacter xylinum (*A. xylinum*)	Investigating DEP micro-weaving to align BC	0.25 V/cm - 1.0 V/cm DC electric fields in a 19 mm long, 500 µm deep PDMS encased microfluidic chamber using Platinum microelectrodes	BC is best synthesized under 0.45V/cm in which interwoven strands of nanocellulose fibrils are aligned in the direction of the applied electrical fields	13

Table 3: Review of Published Studies Using Electric Fields and Analyzing Its Effects on *K. xylinus* and its Effect on BC Synthesis. This Table summarizes findings in literate and highlights parameters of interest regarding the use of electric fields on *K. xylinus* and its effect on BC synthesis.

Noteble studies show that it is possible to stimulate BC synthesis using electric fields [9, 19, 13]. For example, the metabolic process for synthesizing BC was observed by incubating samples exposed to an electric field for 12 hours and another sample of BC not exposed to electric fields for 12 hours [19]. Results suggest that BC production under an electric field promotes cellulose synthesis within a 12-hour period at the cathode [19]. A theory is proposed that in the presence of hydrogen, this generated a strong reductive environment that is beneficial to cell growth, however the growth stopped after 12 hours due to the lack of oxygen and accumulation of lactic acid and pyruvic acid (via the TCA cycle) around the 18 hour mark [19]. Since the key component during the phosphorylation of glucose is completed by the enzyme, UDP-glucose pyrophosphorylase, more oxygen is necessary to complete the hydrogen bonds, where a basic fibril structure needs both oxygen and hydrogen to complete the glucose chain. Any suppression in these metabolic pathways (TCA cycle and glucose phosphorylation) suppress BC growth, which suggests that glucose synthesis is suppressed at the anode at the 6-hour time [19]. To resolve this lack of oxygen, another research group was able to state that while the cells are under the influence of an electric field, the electrolysis of water will create enough oxygen in the solution in the chamber for these metabolic pathways to synthesize BC [9].

This same research group took five separate experiments to demonstrate that a BC producing cell can be controlled using DEP in a microfluidic reactor on a nanoscale. By doing so, they can use electric field to create cellulose networks in 3D. To do this, they control the electrokinetic forces on the bacterial cell to produce cellulose patterns in a

static culture from the bottom-up. This demonstrates the potential to control the direction of fiber orientation to put together multiple fiber layers by changing the orientation of the applied electric field for each layer [9]. By running an experiment for 48 hours while guided through the chamber at a velocity of 1 micron/second, they indicate that the nanocellulose fibrils are aligned in the direction of the electric field suggesting that you can manipulate complex fiber orientations [13].

While these studies are similar to what I am trying to achieve, one of the goals of my thesis is to demonstrate that there is potential for the amount of cellulose synthesized to be influenced by manipulating the magnitude of electric fields in microfluidic reactors. This can be visualized and imaged by using fluorescent stains such as Direct Red 23 or Calcofluor White. This is to perform an extensive study by using DEP techniques to understand the frequency response of *K. xylinus* while also inducing higher magnitudes of AC electric fields to potentially promote *K. xylinus* to synthesize BC on a biological level. This can potentially be done by manipulating electric parameters to clarify some unknowns reported in literature.

2.6 Bacterial Cellulose Stains for Imaging – DR 23 and Calcofluor White

For imaging fluorescent images of BC under the microscope, two stains were considered for this study. The first one being Direct Red 23 (DR 23), also formerly known as Pontamine Fast Scarlet 4B, which is purchased in the form of a powder from Sigma Aldrich known for specifically staining cellulose. The second one being Calcofluor White, which is purchased in the form of a liquid from Sigma Aldrich known

for staining cellulose and chitin in cell walls. Several published studies have compared the two stains for its specificity for staining BC [28, 29, 30, 31, 32]. While both are viable options for staining, it was found that DR 23 binds and stains more specifically to cellulose compared to Calcofluor White [28, 30]. In published studies, DR 23 shows fluorescence for individual cellulose fibers versus the undisguisable bundles within the cell wall when compared to Calcofluor White [28,31]. When cellulose is present, DR 23 has an excitation and emission wavelength of 535 nm and 595 nm, respectively suitable for fluorescent microscopy [28]. Once of the long-term goals for this project is to use DEP techniques for individual cellulose fiber studies, therefore, DR 23 will be used for its specificity towards BC cellulose.

CHAPTER THREE

THEORETICAL BACKGROUND

3.1 Electrical Polarization

Electrical polarization is when a high electric field separates the center of a positive change and the center of a negative charge in a particle or material [20]. However, cells respond differently to electric fields due to their own polarity, the media they are suspended in, and their own biology (i.e. shape and size, biochemical processes, etc.). A cell can polarize and change in response to various chemical, electrical, mechanical, or other physical stimuli [5]. Different magnitudes of polarization can arise from techniques such as DEP, electroporation, and electrical lysis.

3.2 Dielectrophoresis (DEP)

DEP is a phenomenon in which a force is exerted on a polarizable particle of interest when it is under a non-uniform electric field [3]. This dielectrophoretic force can either be positive or negative and depends on the gradient of the electric field and the frequency. For my thesis, particle of interest is the bacterium *K. xylinus.* Using DEP as a technique enables selective manipulation of a bacterial cells using the nonuniform electric field with the induced dipole moment of the cell [9]. The force exerted on this bacterium will depend on the bacterium's electrical properties, shape and size, and

medium. To understand the bacterium's response to the electric field, parameters such as voltage and frequency will be manipulated to observe cellulose synthesis under and electric field. By manipulating these parameters, we hypothesize that we can select and manipulate the growth of cellulose.

This phenomenon was first introduced by Pohl [3] where particles of interest move towards the direction of the electric field gradient. Depending on if the particles move towards the highest electric field (positive DEP) or are repelled away from the electric field (negative DEP), depends on the particle's polarizability in a suspended medium. This DEP force for a spherical shaped particle in a medium m, can be determined by using Equation 1,

$$F_{DEP} = 2\pi\varepsilon_m r^3 Re[f_{cm}]\nabla E_{rms}^2 \tag{1}$$

where, ε is the permittivity of the medium, r is the radius of the cell, ∇E is the gradient of the electric field, and $Re[f_{cm}]$ is the Clausius-Mossoti factor. The Clausius-Mossoti factor can be determined by using Equation 2,

$$f_{cm} = \frac{\varepsilon_p^* - \varepsilon_m^*}{\varepsilon_p^* - 2\varepsilon_m^*} \tag{2}$$

The Clausius-Mossoti depends on the complex permittivity of the medium ε_m^*, and the particle ε_p^*. The complex permittivity is related to the permittivity ε, and the conductivity σ, which can be determined by using,

$$\varepsilon^* = \varepsilon - \frac{j\sigma}{2\pi f} \tag{3}$$

where, f is the frequency of the electric field. The Clausius-Mossoti factor in Equation 3 depends on the frequency, and due to this, it can take positive and negative values for different frequencies of the electric field. This results in the DEP force either being positive (towards the electric field gradient) or negative (against the electric field gradient). To get this polarity in $Re[f_{cm}]$ is obtained by taking the difference between complex permittivity of the media and the bacterial cell. By using a high conductivity of suspending media, this leads to a complex permittivity that is significantly higher than that of the bacterial cell resulting in negative DEP. The opposite effect is true for positive DEP, which is when the complex permittivity of the bacterial cell is higher than that of the suspending media. This complex permittivity is dependent on the bacterial cell membrane properties (i.e. surface area, thickness), volume, nucleus size, and cytoplasm (i.e. ions within the cytoplasm).

By knowing these preliminary equations, we can manipulate the DEP force by optimizing parameters such as the electric field gradient, $Re[f_{cm}]$, and the particle itself. The electric field gradient can be increased by increasing the voltage between the electrode arrays or by decreasing the distance between the electrode arrays. For the opposite effect, the voltage is decreased and the distance between the electrode arrays is spaced further apart. The $Re[f_{cm}]$ is manipulated by increasing or decreasing the frequency allowing us to adjust the DEP response for a specific particle. Since my thesis focuses on *K. xylinus* as my particle of interest, the particle itself cannot be changed. However, depending on the size of a particle, conductivity and permittivity, and

frequency, the DEP force can be manipulated such that we can maximize trapping at the leading edges of the electrodes.

3.2.1 DEP Force on a Particle

As mentioned, the DEP force is dependent on the particle's polarizability under a non-uniform electric field. Therefore, the polarization of a particle must be considered by calculating the net dipole force that is induced on a particle, as shown in Equation 4,

$$F = qE(r + d) - qE(r) \tag{4}$$

where, the electric field $E(r + d)$ can be expanded depending on the vector position of the particle r using the Taylor series expansion. The d, which is the distance of two opposite charges, simplifies the Taylor series expansion to only the zero term and first term giving you Equation 5,

$$F = (qd \cdot \nabla)E = (p \cdot \nabla)E \tag{5}$$

Since $p = qd$, where p is the dipole moment and +q/-q (positive or negative charge), this allows you to calculate the electric potential of the dipole as shown in Equation 6.

$$\Phi = \frac{pcos\theta}{4\pi\varepsilon r^2} \tag{6}$$

By using this equation, the induced nonuniform electric field of a dipole moment of a particle, p can be calculated. These Equations 5 and 6 can be compared to further investigate the electrical potential using the single-shell model.

3.2.2 The Shell Model

Bacterial cells have multiple layers, each with their own respective electrical properties due to the cell membrane properties (i.e. surface area, thickness), volume,

nucleus size, and cytoplasm (i.e. ions within the cytoplasm). Due to this, the single shell model is used to simply the analysis of nonhomogeneous particles, as shown in Equation 7,

$$Re[f_{cm}] = \left(\frac{\varepsilon_{eff} - \varepsilon_m}{\varepsilon_{eff} + 2\varepsilon_p}\right) \tag{7}$$

where, ε_{eff} is the effective complex permittivity of a cell given by,

$$\varepsilon_{eff} = \varepsilon_{mem} \frac{\left(\frac{r_{outer}}{r_{inner}}\right)^3 - 2\frac{\varepsilon_{cyt} - \varepsilon_{mem}}{\varepsilon_{cyt} + 2\varepsilon_{mem}}}{\left(\frac{r_{outer}}{r_{inner}}\right)^3 - \frac{\varepsilon_{cyt} - \varepsilon_{mem}}{\varepsilon_{cyt} + 2\varepsilon_{mem}}} \tag{8}$$

where, r_{inner} and r_{outer} are inner and outer diameters of the cell and ε_{cyt} and ε_{mem} are complex permittivity of cytoplasm and membrane, respectively. This model simplifies the cytoplasm, nucleus, and cell membrane into three domains. These shell models are used to model complex dielectric properties of cells [10]. For example, mammalian cells are typically modeled as a one-shell model to account for a cell membrane containing a cytoplasm. Whereas plant cells and certain microorganisms are modeled using a two-shell model to account for the presence of a cell wall enclosing the membrane and the cytoplasm. Since *K. xylinus* is very a small bacterial cell, DEP forces exerted are always positive and more dependent on the solution conditions rather than aspects of the cell itself due to the double layer and its interface with the medium having similar characteristics [11]. Therefore, the properties of the media are a contributing factor used to determine the AC electrokinetic response of the bacterial cell.

3.3 Electroporation

Electroporation is a technique used in biological cell studies that applies a high voltage electric field near cells, which can generate nanopores in the cell membrane [14]. By varying the intensity and duration of the electric field this can create the potential insert biological samples into cells or release intercellular contents from the cell. There are conventional electroporation devices that can perform this technique, but microfluidic electroporation devices have the potential to promote higher cell viability, higher transfection rates, low sample contamination, and smaller Joule heating effects [14].

There is a theory called membrane permeabilization specific for microfluidic electroporation that will be discussed for this study. As mentioned, the cell membrane has pores due to an electric field. This theory looks at the minimum amount of energy that is acceptable to uniformly polarize the membrane for this phenomenon. [14]. Based on this theory, there are hydrophobic and hydrophilic pores where hydrophobic pores indicate the potential for water-insoluble substances to repel, and hydrophilic pores indicate the potential for water-soluble substances to attract based on the lipid bilayer of the cell [14]. There are equations to calculate pore energy are represented as,

$$hydrophobic\ pore\ energy: U(r) \approx E_* \left(\frac{r}{r_*}\right)^2 - \frac{1}{2h}(\varepsilon_w - \varepsilon_m)V_m^2 \pi r^2 \quad (9)$$

$$hydrophilic\ pore\ energy: E(r) \approx \beta \left(\frac{r_*}{r}\right)^4 + 2\pi\gamma r - \sigma\pi r^2 - \int_{r_*}^{r} F(r', V_m)dr' \quad (10)$$

Table 4 describes the variables of the equation in detail. When r < r_* pores are hydrophobic and when r > r_* pores are hydrophilic.

Variables	Explanation
$U(r)$	Hydrophobic pore
$E(r)$	Hydrophilic pore
r	Pore radius
r_*	Radius between hydrophobic and hydrophilic pores
E^*	Threshold pore energy at r_*
h	Membrane thickness
ε_w	Permittivity of the water
ε_m	Permittivity of the membrane
V_m	Transmembrane potential
β	Constant
γ	Constant
σ	Membrane tension
F	Electrical Force

Table 4: Variables for Equation 9 and 10 for hydrophilic and hydrophobic pore energy

Based on this information, studies can use this to hypothesize analytical models to address microfluidic cell electroporation. This is done in order to determine the minimum amount of pore energy necessary to stimulate cell electroporation to introduce materials moving in and/or out of the cell via the cell membrane.

3.4 Electrical Lysis

Electrical lysis happens when a high electric field is introduced to a biological cell causing it to break open and disintegrate the plasma membrane.

When biological cells are exposed to an electric field, there is a transmembrane potential created along the cell membrane. Once this potential reaches a certain voltage (which vary depending on the cell), this creates the pores along the membrane as mentioned in Section 3.3. Once it exceeds this threshold, the cell will release its

intracellular contents or if it does not exceed the threshold, then the cell will reseal its pores. However, if this threshold is exceeded exponentially, this will cause a breakdown of the cell membrane leading to electrical lysis.

DC electric fields are more susceptible to this as the threshold is around 1 V [14]. Therefore, we use AC electric fields to minimize adverse effects to a biological cell with a target magnitude of less than 10^5 V/m [14, 43].

3.5 Electrochemical Stability of Titanium

Titanium was analyzed as an electrochemical capacitor compared to other metal oxide capacitors. An incentive to use titanium was due to its biostable and biologically compatible properties when using it on biological microorganisms [39, 40]. It is also corrosion resistant to its physiological environment allowing multiple uses in various types of solutions giving it desirable robustness in microfluidic use [39]. Studies have also shown that titanium electrochemical capacitors have enhanced cell viability and cell adhesion for long-term culture use in low conductive media [40]. These reasons make using titanium desirable for this study's application.

CHAPTER FOUR

MATERIALS AND METHODS

4.1 Culture of *K. xylinus* and Experimental Media

K. xylinus was purchased as a freeze-dried culture from American Type Culture Collection (ATCC), which specializes in providing standard reference microorganisms, cell-lines, and other materials. HS Culture media was prepared as follows. 0.5% yeast extract (w/v), 0.5% peptone, 0.27% Na_2HPO_4 (w/v), and 0.15% citric acid (v/v) were mixed and then autoclaved. After autoclaving, 2.0% dextrose (w/v) was added to complete the media. The pH was adjusted using 1.0 M acetic acid solution to a pH of about 5 – 5.5. The media was then split in 50 mL fractions in separate tubes and refrigerated at 4°C for future use.

K. xylinus cultures were incubated at a temperature of 28°C in 100% HS media for 48 hours for a target density of roughly $1x10^7$ cell/mL. The culture was grown in a static environment to produce undisturbed, light-yellow, and opaque layers of BC as shown in Figure 4. To pass the culture for cell resuspension, the cells were was shaken to break apart the BC and evenly distribute the cells resulting in 333 µL of cells, 267µL of dextrose, and 5mL of 100% HS media in a newly suspended 15 mL culture tube.

Figure 4: Image of *K. xylinus* culture grown in 15 mL tubes. The top opaque layer indicates a healthy layer of BC forming on top.

The experimental sample was composed of as follows – 5mL of *K. xylinus* mixed with 4.5 mL of an optimized DEP buffer solution composed of 8.6 wt% sucrose, 0.3 wt% dextrose and 0.1 wt% bovine serum albumin to obtain a concentration of about 10^7 cells/mL. The sample was prepared in a 5 mL syringe. Hence, the electrical properties of the experimental sample were a cell concentration of 10^7 cells/mL, a pH of roughly 5 – 5.5, and a media conductivity of 504 µS/cm.

Cells were then pelleted through centrifugation for 5 minutes at 5000 rpm and then resuspended into fresh DEP buffer solution. This centrifugation and re-suspension protocol were repeated three times to ensure complete removal of any remaining HS culture media. The final resuspension volume inside the syringe consisted of 4.5 mL of DEP media and 500 µL of bacterial cells.

4.2 Computational Modeling of the Electric Field Around Microelectrodes

A few variations of microelectrode designs were considered for this study. The goal was to create punctual locations to observe the electric field to promote positive DEP for *K. xylinus* enrichment to facilitate the observation of BC synthesis at specific/pre-determined locations. Our research group has tested several microelectrode designs such as triangular, square, semicircular, etc. [42]. However, semicircular electrodes provide weaker electric field gradients versus concentrated/punctual points to safely trap *K. xylinus* and prevent cell lysis [43]. Due to this, the semicircular microelectrode design was chosen for this study as shown in Figure 5.

Figure 5: Semicircular microelectrode design chosen.

The software ANSYS Electronics Desktop running on a Lenovo H50-55 with an AMD A10 780 CPU and 12 GB of RAM was used to model the electric field (*E)* and the squared of the electric field gradient (∇E^2) using built in Maxwell 2D electrostatic solvers. The magnitude and spatial distribution of the electric field were modeled for semicircular microelectrodes at four different values of polarization voltage at 1 V_{pp}, 2 V_{pp}, 5 V_{pp}, and 7 V_{pp}. This was done to assess the relation between the polarization voltage and the resultant electric field, and gradient, for the semicircular electrode geometry. Such study was important to ensure the applied field did not lead to lysis of *K. xylinus*. Depending on the selected voltage, the electric field gradient was modeled to estimate the strength of positive DEP force.

For the simulation, a few parameters were assumed. The Ti-microelectrodes were set at the material of choice. Since the voltage is applied directly to the Ti-microelectrodes for our experiments, we assume that there is no loss of resistance going from the function generator to the Ti-microelectrode chip. Since the design of the microelectrodes are symmetrical, it can be assumed that the resultant electric field for one electrode is the same for all electrodes across the entire array of the Ti-microchip. The medium suspension is set as distilled water with an electric conductivity of 504 µS/cm to simulate the conductivity of our experimental medium. Figure 6 highlights the setup of the simulation indicating important set parameters.

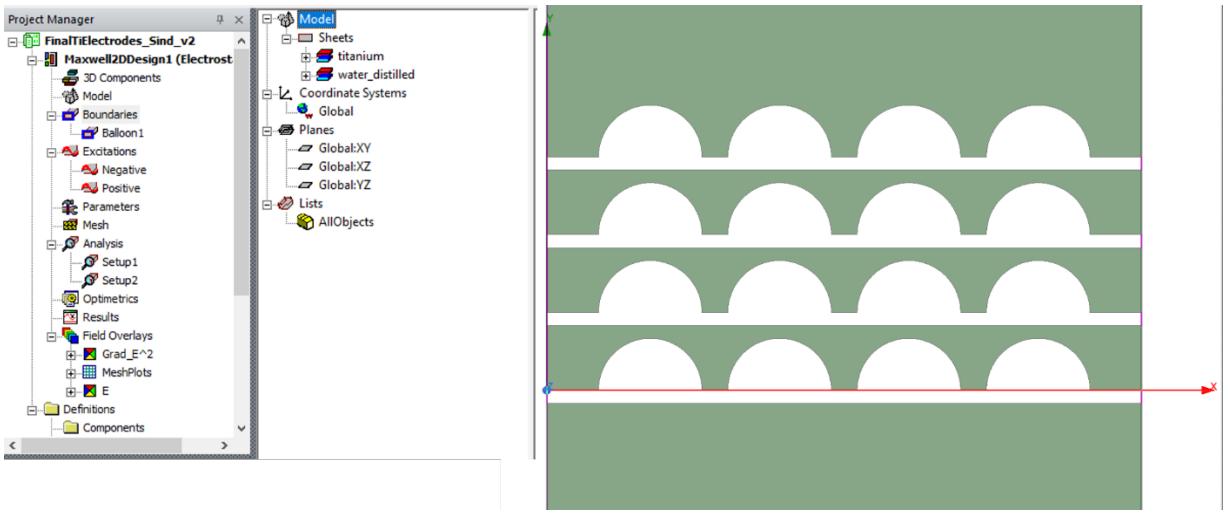

Figure 6: Screenshot of the ANSYS workspace highlighting the boundary conditions and Ti-microelectrode design with specific set parameters.

The results of the simulation are detailed in Section 5.1 in the Results section. Based these results and how the electric field behaved after testing various voltages for the Ti-microelectrodes, unique regions of interest were drawn as indicated in Figure 7 by using the center-to-center distance of the semicircle roughly space 300 µm apart. Regions

1, 2, 3, 4 and 5 indicates potential areas where the simulation *K. xylinus* can experience positive DEP trapping at the leading edges of the electrode. Region 6 is to account for any free-floating cells that are suspended in the medium that may experience effects from the electric field. Region 4A indicates the strongest electric field where we think the greatest number of bacterial cells will be trapped at the leading edges of the electrode. Hence, the most important region for studying the potential of BC synthesis.

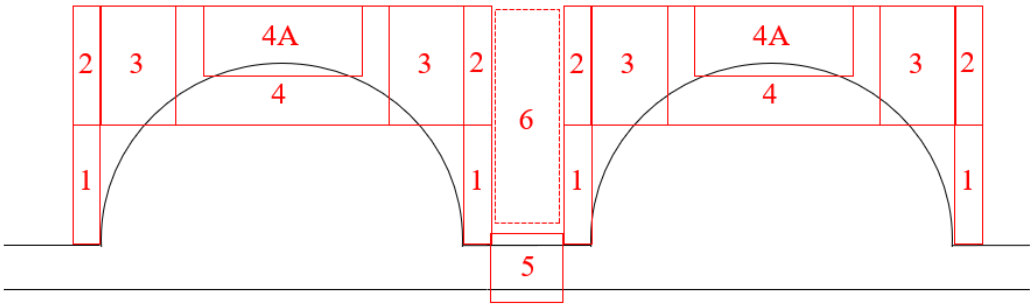

Figure 7: Unique regions of interest drawn for Region 1, 2, 3 4, 4A, 5, and 6 based on the ANSYS simulation results and using the center-to-center distance of the semicircle. This is to account for all potential bacterial cells trapped at the leading edges of the Ti-electrodes. Region 4A indicates the strongest electric field for studying BC synthesis.

4.3 Device Fabrication

A couple of devices were fabricated in a cleanroom using photolithography techniques to determine which microelectrodes would be ideal to use for experiments. These fabrication processes are described in detail in Section 4.3.1 and 4.3.2. Ti- and ITO- microelectrodes were considered for this study. Ti based microelectrodes were used as a starting point since our research group had already done extensive experiments featured in published work [42]. The ITO microelectrodes were intended to be used at the

Clemson Light Imaging Facility (CLIF) as they are transparent allowing for high resolution confocal microscopes to be used, which possess the potential to see BC nanofibers. Currently, the microscope featured in our lab takes images from the top, but CLIF microscopes take image from the bottom, therefore, the need for transparent microelectrodes. Therefore, preliminary results will be obtained using the Ti-chip for proof of concept and the ITO-chip will be used for further work at CLIF.

4.3.1 Titanium-Microelectrode Devices

A previously developed protocol from our research group was used to fabricate the devices [42]. The titanium electrodes were fabricated on a silicon oxide surface through a lift-off process, which is illustrated in Figure 8. Silicon wafers (100 mm thick) with a 500 nm-thick thermal oxide went through an oxygen plasma treatment process at 20 μTorr for 15 seconds. Figure 8B shows a layer of LOR resist was spin coated onto the silicon substrate at 2000 rpm for 45 seconds and then hard baked on a hotplate at 150°C for 150 seconds. In Figure 8C, a layer of AZ701 photoresist was spin coated at 3000 rpm for 45 seconds on top of the LOR, baked at 110 °C for 75 seconds, and then exposed to a light with λ= 365 nm and intensity of 6 mW/cm^2 for 20 seconds to generate the pattern. Another post exposure bake was done on a hotplate at 110 °C for 60 seconds. The exposed AZ701 and LOR layers were then immersed in a 2.3% tetramethylammonium hydroxide/97.7% water bath to develop the AZ layer and underetch the LOR giving you the pattern shown in Figure 8D. The wafer was immersed for 2 minutes followed by a visual inspection to ensure the AZ701 layer's underetch was about 2 μm. Once rinsed and dried, the wafer was transferred to a metal evaporator to deposit 350 nm of Ti as shown

in Figure 8E. After the deposition process, the wafer was immersed in NMP (1-methyl-2-pyrrolidone) remover to dissolve the AZ and LOR layers and effectively lift-off the Ti from undesired regions of the substrate giving the final device as shown in Figure 8F.

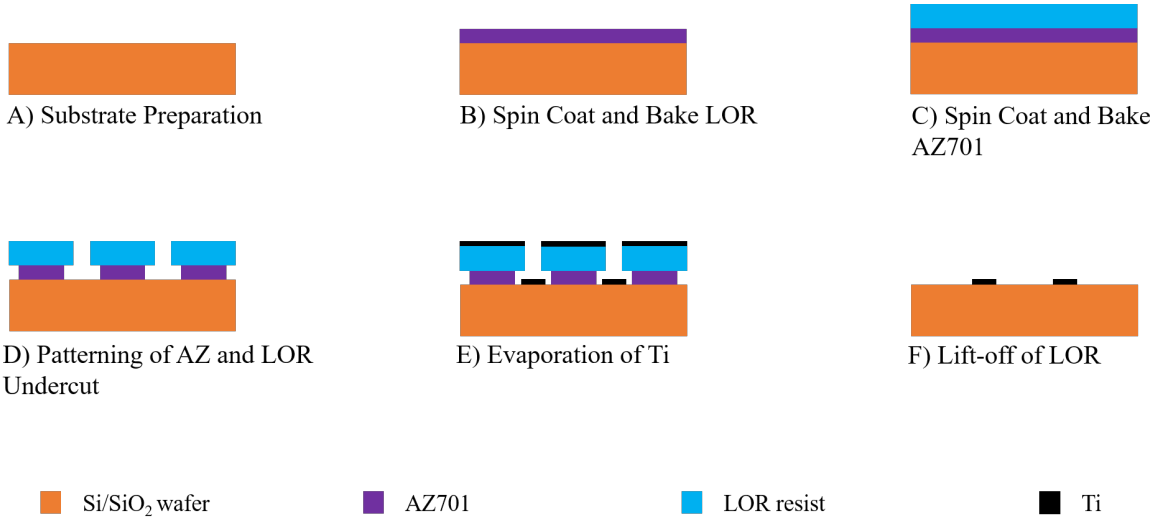

Figure 8: Ti-Microelectrode Device Fabrication Process

4.3.2 Indium Tin Oxide (ITO)-Microelectrode Devices

The ITO electrodes were fabricated on a 7 Ohm/sq ITO coated polished silicon glass wafer (1.1 mm and 0.7 mm thick) though a life-off process illustrated in Figure 9. These were purchased from universitywafer.com. The wafers went through an oxygen plasma treatment process at 10 µTorr for 2 minutes. Figure 9B shows a layer of SU-8 photo resist that was spin coated onto the substrate at 3000 rpm for 80 seconds and then soft baked on a hotplate at 95°C for 6 minutes. In Figure 9C, a mask was used where the wafer was exposed to a light with λ= 365 nm and a dose of 180 mJ/cm^2 for 20 seconds to generate the pattern followed by a post-exposure bake at 95°C for 2 minutes. Figure 9D shows the wet etching process where the wafer was submerged in 1.0 M oxalic acid for

about 75 minutes followed by visual inspection to ensure minimal under etch in the ITO layer. Appendix A indicated the oxalic acid's etch rate results. The final step is the removal of the SU-8 photoresist layer using a sonicator bath. The wafer was placed in a beaker was filled with NMP (1-methyl-2-pyrrolidone) remover and placed in the bath at 75°C for 1 hour to dissolve the SU-8 layer.

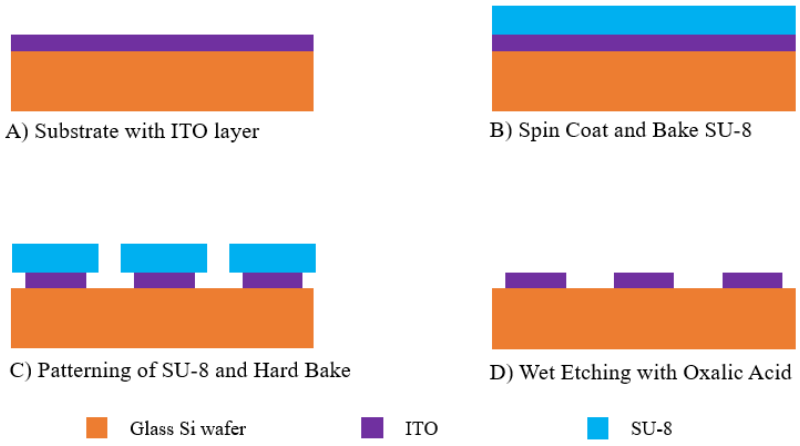

Figure 9: Indium Tin Oxide (ITO)-Microelectrode Device Fabrication Process

4.3.3 Finalized Device

The microfluidic DEP device used to start this study featured Ti-microelectrode arrays. The Ti microelectrode array way combined with a 1.8 mm-wide and 32 mm-long channel was patterned from 127 µm-thick sheet of double-sided pressure sensitive adhesive, or PSA (Switchmark 212R, Flexcon, Spencer, MA, USA), using xurography and adhered to a previously machined polycarbonate (PC) piece [44]. The finalized DEP chip was assembled manually by combining the PC/PSA arrangement on top of the Ti-microelectrode array and sealed by a rolling press. Figure 10 features the finalized Ti-

chip with the PC/PSA arrangement mounted on top along with a zoomed in view under the microscope and a cross-sectional view.

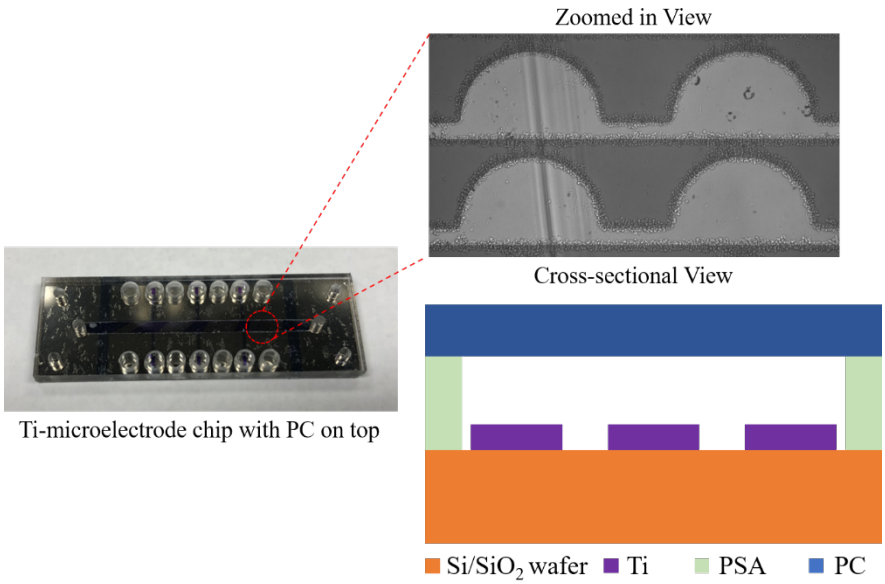

Figure 10: Finalized Chip

A top view of the finalized Ti-chip is shown in Figure 11 featuring 192 (6 rows x 32 columns) semicircular Ti-microelectrodes each spaced 300 µm based on the center-to-center distance of the semicircles with a radius of 30 µm (note – drawing in the figure is not drawn to scale). However, only 8 electrodes were in the field of view under the microscope for analysis.

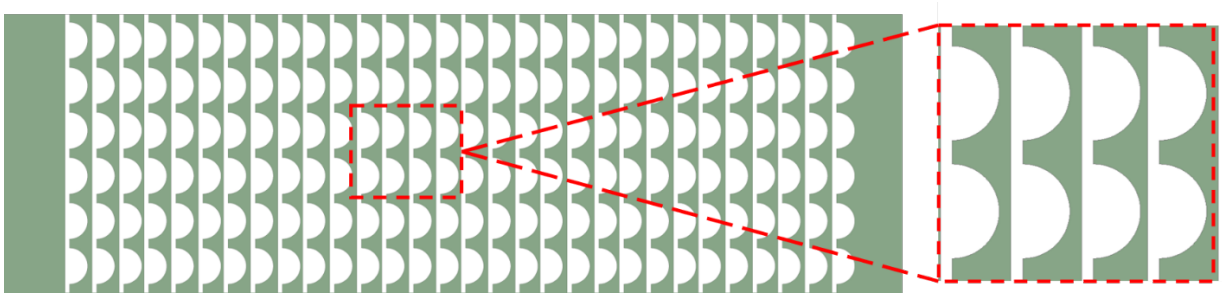

Figure 11: Top View of the Ti-microchip featuring 6 rows x 32 columns of semicircular microelectrodes. Each electrode is spaced 300 µm apart based on the center-to-center distance of the semicircle. The field of view features only 8 electrodes for analysis while taking live cell images under the microscope.

4.4 Experimental Platform and Protocol to Characterize Frequency Response and Bacterial Cellulose Synthesis Under an Electric Field

An overview of the experimental setup is shown in Figure 12 and will be described in detail. Ti-microelectrode arrays were used for the microfluidic DEP experiments. The Ti-chip was connected to a BKPrecision 4040B function generator to generate the desired voltage and frequency.

This mixture in the 5 mL syringe was injected to the chip using a FusionTouch 200 by Chemyx to flow the experimental sample into the microfluidic chamber. Once stabilized in the chamber, images can be acquired.

The Ti-chip was placed stationary in the microfluidic chamber under an Andor Zyla Camera coupled to a LV100 Nikon Eclipse Microscope at 20x magnification to facilitate image acquisition for the experiments for cell characterization and the cellulose synthesis time study. Images were taken and saved onto a computer for later image post-processing.

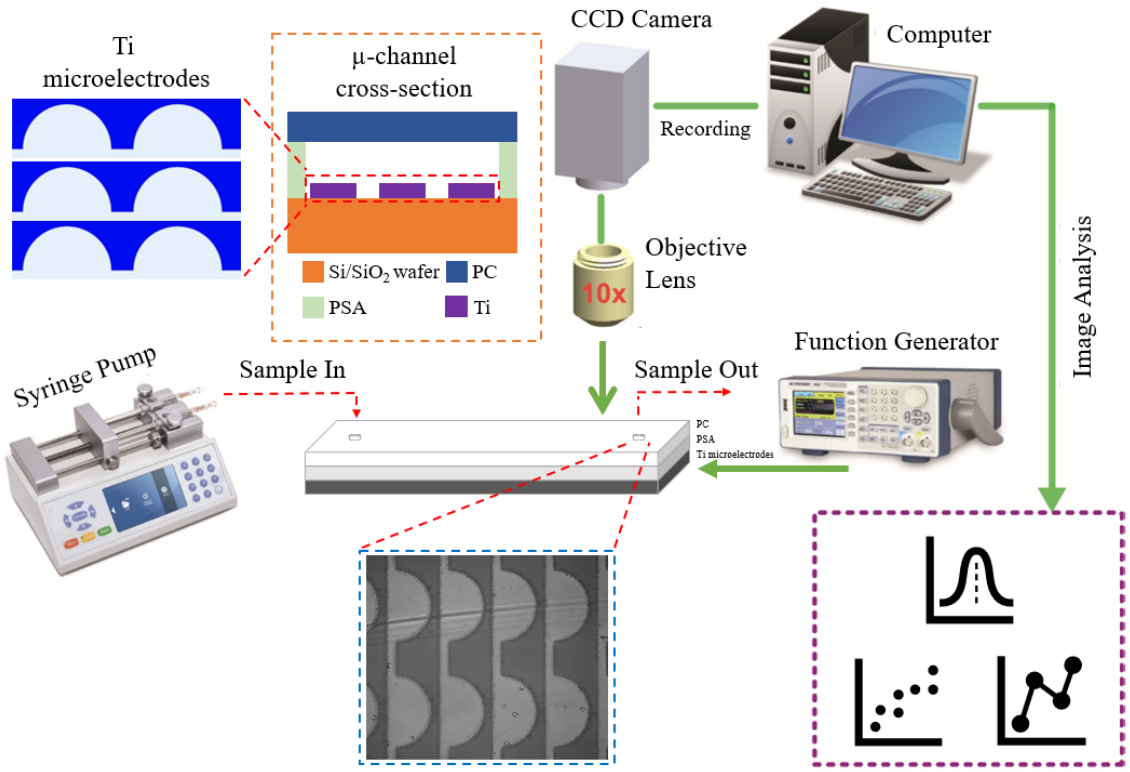

Figure 12: Experimental Set-up Overview

The experiment protocol will be broken up into two sections. One for cell frequency characterization and the second one for the cellulose synthesis time lapse study. Figure 12 and Section 4.4 earlier describes an overview of the general experimental setup.

4.4.1 Experimental protocol – Frequency Characterization

The experimental protocol did not feature any flow and all experiments were done in stationary conditions. First 25-50 μL of the experimental sample was injected into the microfluidic chamber of the device using the FusionTouch 200 by Chemyx. The sample was given time to stabilize for about 10 minutes at 0.25 – 10 MHz at a polarization

voltage of 5 V_{pp} using a BKPrecision 4040B function generator to give any free-floating cells a chance to be migrate/attach to the leading edges of the microelectrodes.

Using the Andor Zyla Camera coupled to a LV100 Nikon Eclipse Microscope, a video recording of the experiment was started. After 10 seconds, the function generator was turned off to study and observe the bacterial cell's response for a total duration of 90 seconds. All videos were analyzed using ImageJ for post-processing.

4.4.2 Experimental Protocol – Bacterial Cellulose Synthesis

The samples of *K. xylinus* for this study was prepared very similarly as described in Section 4.4.1. After the centrifugation and re-suspension protocol, 5 µL of 0.01% w/v DR 23 stain was added and then prepared in a 5 mL syringe. The final resuspension volume inside the syringe consisted of 4.5 mL of DEP media, 500 µL of bacterial cells, and 5 µL of 0.01% w/v DR 23 stain.

The experimental protocol did not feature any flow and all experiments were done in stationary conditions. First 50-100 µL of the experimental sample was injected into the microfluidic chamber of the device using the FusionTouch 200 by Chemyx. The sample was given time to stabilize for about 30 minutes at 750 kHz using a BKPrecision 4040B function generator to give any free-floating cells a chance to be migrate/attach to the leading edges of the semicircular microelectrodes.

Using the Andor Zyla Camera coupled to a LV100 Nikon Eclipse Microscope, images of the brightfield were taken at Day 0 – Day 14. To take fluorescent images, a 49010 - ET - R&B Phycoerythrin/mOrange/mKO Nikon filter made by Chroma Technology Corporation was used to image the Direct Red 23 fluorescent stain specific

for BC from Day 0 – Day 14. Every 14 days, images were taken every 48 hours to observe *K. xylinus* and cellulose synthesis at polarization voltages of 1 V_{pp}, 2 V_{pp}, and 5 V_{pp}. Figure 13 depicts how the pre-defined regions appear for post-processing in ImageJ with an image taken from under the microscope.

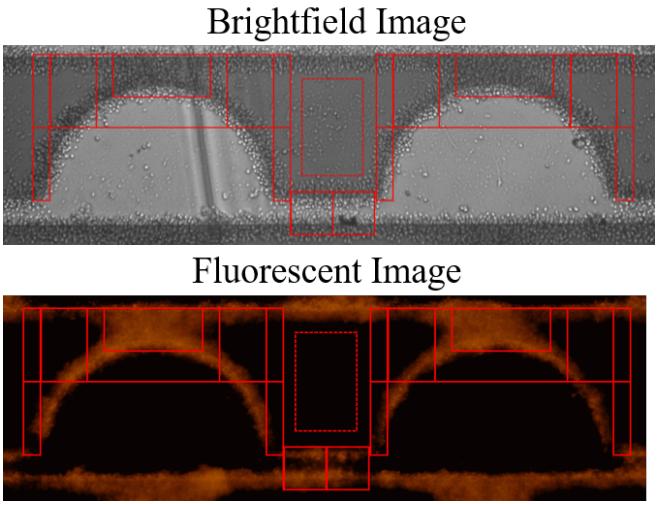

Figure 13: Brightfield and Fluorescent image view under the microscope with regions of interest overtop for post-processing in ImageJ

4.5 Data Acquisition

The data analysis for this thesis will be broken up into two sections.

4.5.1 Frequency Characterization

The DEP response of the *K. xylinus* was characterized based on the percentage of the bacterial cells that were attracted to the electrode at the time mark of 15 seconds. The percentage of attracted bacterial cells was calculated using Equation 11 by comparing the total number of bacterial cells visible in the field of view at 90 seconds, or $I_{t=90}$, to the

number of bacterial cells that were attached to the electrode in the field of view at 15 seconds, or $I_{t = 15}$,

$$\left[\frac{(I_{t = 90} - I_{t = 15})}{I_{t = 15}}\right] \times 100 \quad (11)$$

This analysis was done for three videos per each of the frequencies investigated in the range of 0.25 – 10 MHz. A higher percentage of attached cells was assumed to indicate a stronger positive DEP response induced on *K. xylinus*.

4.5.2 Bacterial Cellulose Synthesis

The ability to enrich the *K. xylinus* in specific locations was measured by monitoring the number of them over time in unique and pre-defined regions of interest for each of the 8 electrodes, as illustrated in Figure 7. Bacterial cell intensity was measured for each region and reported as a percentage increase or decrease in bacterial cells from time t = day 0 to t = day 14 for the brightfield and fluorescent images by using ImageJ. The average intensity was plotted for each of the defined regions every two days to determine their bacterial cellulose synthesis potential. The percent intensity for each region was calculated as a percentage change in the number of bacterial cells from time t = day 0 to time t = day 14 for brightfield and fluorescent images using Equation 12,

$$\left[\frac{(I_{t = Day\ X} - I_{t = Day\ 0})}{I_{t=Day\ 0}}\right] \times 100 \quad (12)$$

where, $I_{t = Day\ 14}$ is the average intensity of bacterial cells in at day 14 and $I_{t = Day\ 0}$ is the average intensity of bacterial cells at day 0 for the same region. This consideration was used as a method to facilitate direct observation of the bacterial cells in specific locations

based on the electric field from the simulations done in ANSYS. In this study, positive values in intensity percentage indicate a tendency for bacterial cells to migrate towards the region of interest, thus promoting the potential for cellulose synthesis.

CHAPTER FIVE

RESULTS AND DISCUSSION

5.1 Computational Modeling Results

This first section will feature the simulation results based on the modeling of the electric field in ANSYS with the chosen semicircular microelectrodes. The panel of figures in Figure 14 and Figure 15 below features the magnitude and distribution of the electric field gradient in the microfluidic device at different polarization voltages at 1 V_{pp}, 2 V_{pp}, 5 V_{pp}, and 7 V_{pp}. Due to the symmetrical design for each electrode, the distribution of the electric field will be the same across all electrodes in the Ti-microelectrode array. However, only four electrodes will be featured in the panel of figures.

Figure 14 results show that the magnitude of the electric field is directly proportional to the voltage. The goal is to target an electric field magnitude of less than 10^5 V/m for optimal cell viability while exposed to strong AC fields in the chosen frequency range of the experiments [43]. This is to minimize the adverse effects due to long-term exposure to electric fields to maintain optimal cell viability of *K. xylinus* as best as possible. Results of 7 V_{pp} are shown to ensure the magnitude of the electric field remains less than 10^5 V/m due to long-term exposure.

Based on these results, 1 V_{pp} was chosen to start the experimental study featuring a magnitude of approximately 11.6 kV/m. The experiments will feature long term

exposure to AC fields all the way up to 5 V_{pp} ensuring that the magnitude of the electric field will remain within 10^5 V/m as given by the simulation results. This is to limit potential adverse effects, which results suggest could happen at approximately 7 V_{pp} as indicated in the orange – red regions.

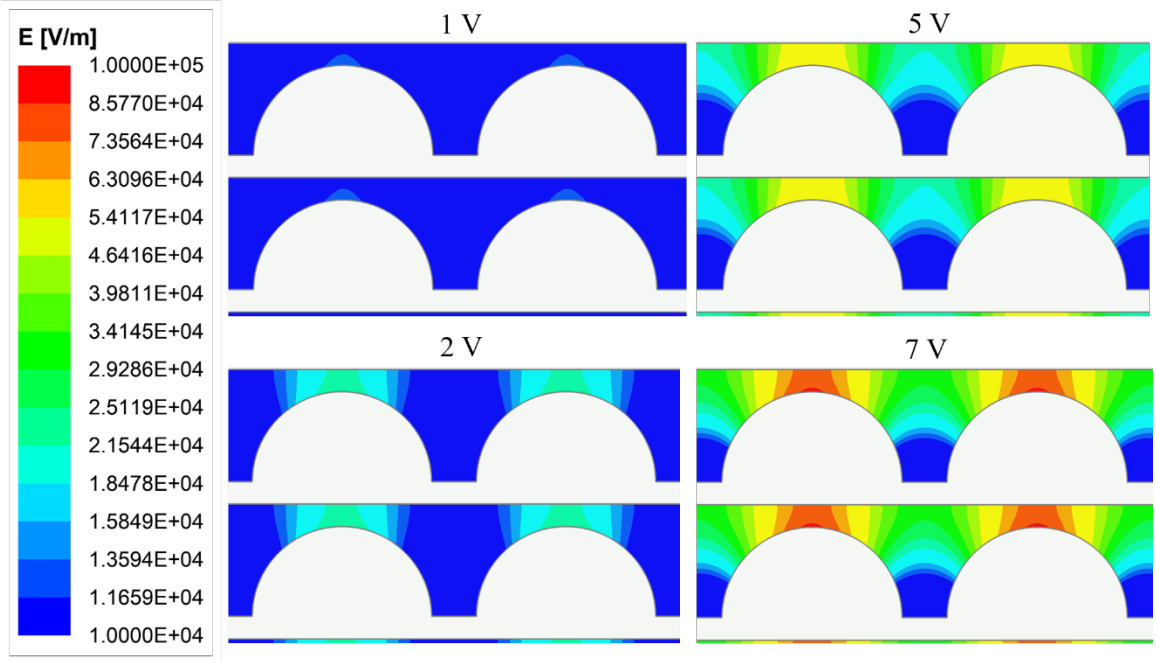

Figure 14: Modeling of the Electric Field for the Ti-microelectrodes at different voltages. The modeled media around the electrodes was water with an electrical conductivity of 504 µS/cm. The simulations show that the magnitude of the electric field is directly proportional to voltage. By keeping the magnitude less than 10^5 V/m, this ensures optimal cell viability of *K. xylinus* and prevents electrical lysis. The simulations indicate that electrical lysis may start to occur at 7 V_{pp} as shown in the orange-red regions in the figure.

Figures 15 show the modeled distribution of the electric field gradient in the microfluidic device when the Ti chip is polarized at 1 V_{pp}, 2 V_{pp}, 5 V_{pp}, and 7 V_{pp}. In order to induce positive DEP, *K. xylinus* will need to move towards the regions with the highest electric field gradient, which can be shown in the green - yellow regions. Based on this computation model, *K. xylinus* will start to migrate towards the leading edges of the semicircular electrodes starting at 1 V_{pp}. Therefore, reinforcing starting the

experiments at this voltage. Previous experiments have also shown that the bacteria can start to experience positive DEP starting at 1 V_{pp}.

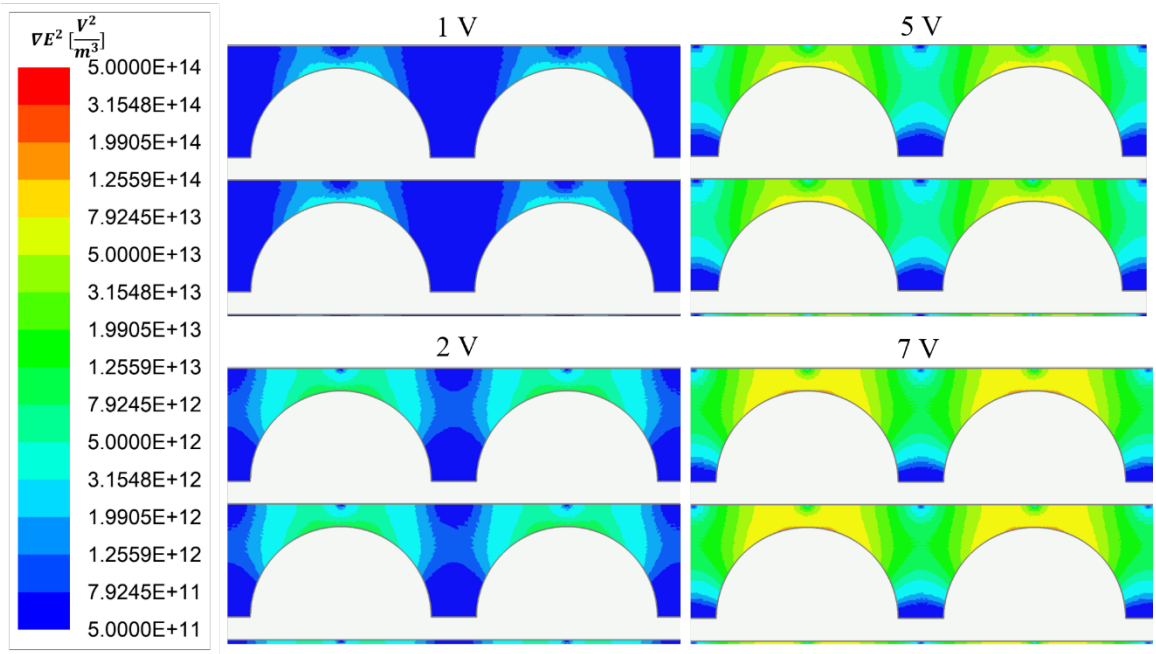

Figure 15: Modeling of the distribution of the Electric Field Gradient in the microfluidic reactor when the Ti-microelectrodes are polarized at 1 V_{pp}, 2 V_{pp}, 5 V_{pp}, and 7 V_{pp}. The modeled media around the electrodes was water with an electrical conductivity of 504 µS/cm. When *K. xylinus* experiences a positive DEP force, they are expected to migrate towards the regions of the highest electric field gradient, as shown in the green-yellow colors in the figure.

5.2 Frequency Response of *K. xylinus* Based on Culture Age

K. xylinus has its own electrical properties depending on its cellular components such as cell size, the membrane, the cytoplasm, and medium it is suspended in. Due to these naturally existing charges, *K. xylinus* can redistribute its charges based on the electric field it is exposed to. This causes cell polarization, the inductance of an electric dipole, and positive (or negative DEP) motion [6]. Due to the cellular components, such as the cell wall, a membrane capacitance is generated, and interacts with the suspending

media, which will facilitate how the cells move in response to an electric field and frequency. Thus, a positive DEP response allows *K. xylinus* to move towards to leading edges of the microelectrodes and negative DEP allows *K. xylinus* to move away from the leading edges of the microelectrodes based on the electric field gradient.

This generates the curves shown in Figure 17, which show the DEP response of *K. xylinus* to an applied voltage at 5 V_{pp} at different frequencies ranging from 250 kHz – 10 MHz. The study was done at 3 different culture incubation times of 24, 48, and 96 hours and repeated three times for each incubation time. The results plot the percent change in intensity over time based on the DEP response of *K. xylinus* at each tested frequency.

An example of the raw data generated is shown in Figure 16. This graph represents the trapping behavior of *K. xylinus* on the Ti-microelectrode over a 90 second time span. The first 10-15 seconds have a minimal change in intensity as the electric field is on. When the electric field is turned off, the change in intensity decreases significantly as any previously trapped bacterial cells are released and cross over the data analysis region. This decrease in intensity is representative of the number of cells that cross over the data analysis region, thus indicating a stronger positive DEP response. The last 40-90 seconds show a stagnant change in intensity as any cells trapped on electrode arrays located upstream of the data analysis region are eluted.

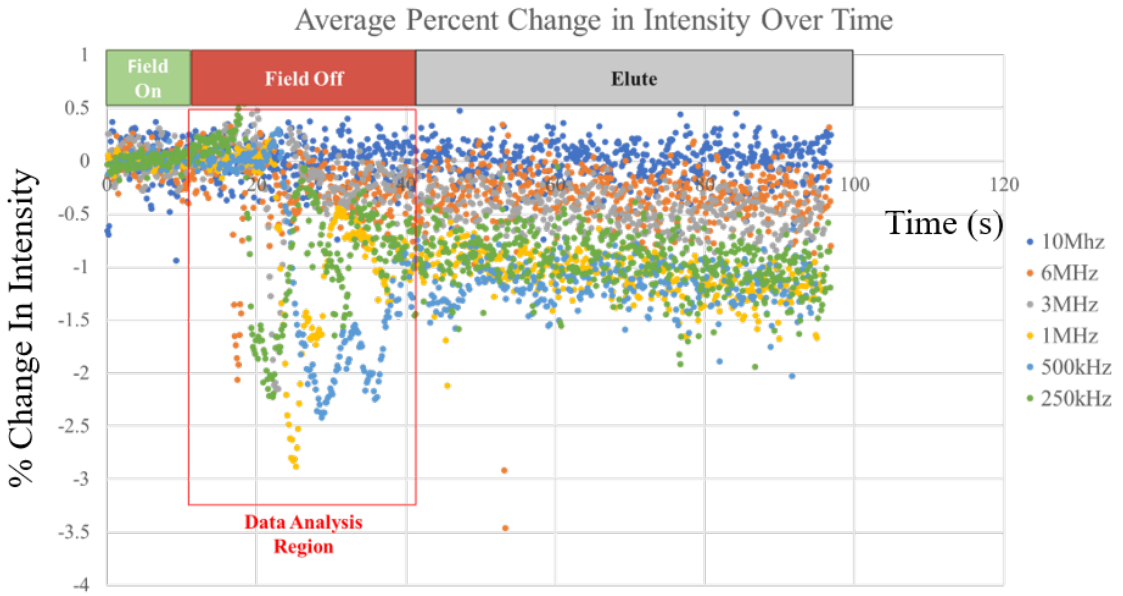

Figure 16: Raw Data for Average Percent Change in Intensity Over Time. This plot represents the trapping behavior of *K. xylinus* on the Ti-microelectrode over a 90 second time span at 5 V_{pp}. The plot indicates important areas such as the 0-10 second mark where the electric field is turned on and the 10-15 second mark where the electric field is tuned off. This 10-15 second mark is the data analysis region to monitor how the bacterial cells behave as it crosses over the data analysis region when the field it turned off as indicated by change in intensity. The last 40-90 seconds show a stagnant change in intensity.

Figure 17 shows that *K. xylinus* exhibited a positive DEP response from 250 kHz to 10 MHz allowing the trapping of bacterial cells at the leading edge of the Ti-microelectrodes. At 5 V_{pp}, a frequency of 500 kHz generated strongest positive DEP force and the highest percent change in intensity for all incubation times (24, 48, and 96 hours). The red line represents 24 hours of incubation, the green line as 48 hours of incubation, and the blue line as 96 hours of incubation. Positive DEP response rapidly declines at roughly 1 MHz.

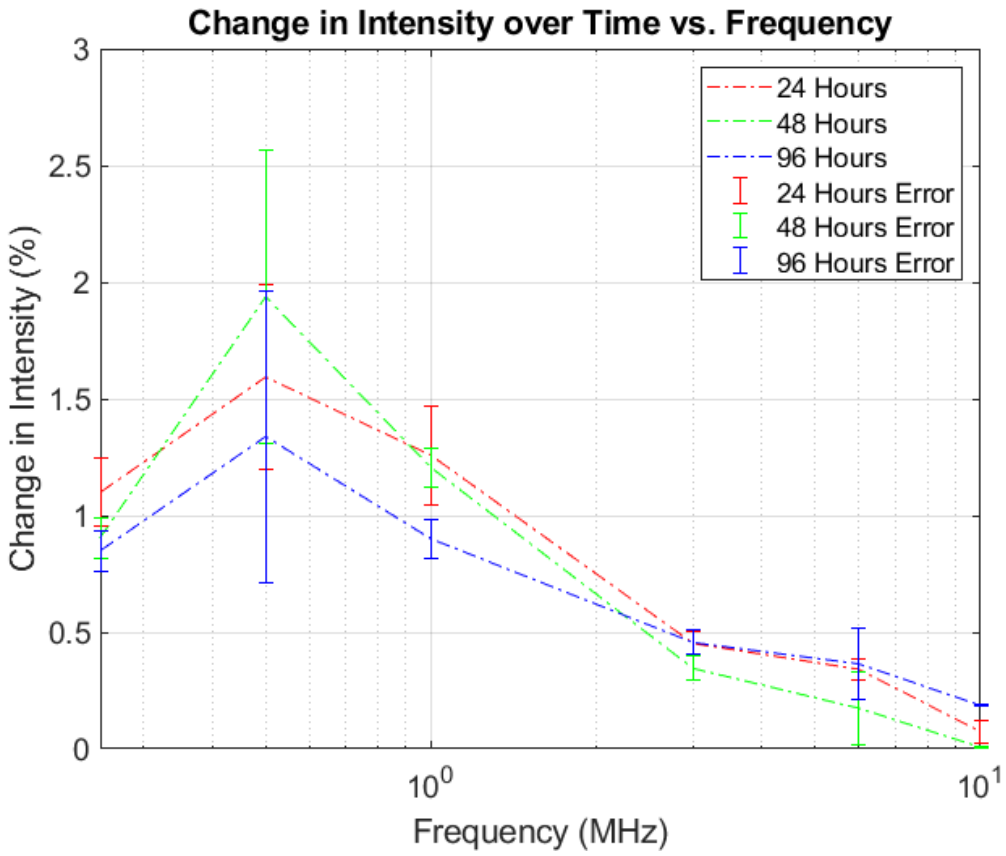

Figure 17: 24, 48, and 96 hour DEP response from 250 kHz to 10 MHz with 500 kHz generating the strongest DEP response and change in intensity.

This similar DEP responses between the varying incubation times (24, 48, and 96 hours) could be due to the bacterial cells maintaining homeostasis. As the cells age, their composition changes due to cell division and its metabolic pathways. However, it is important to note that the *K. xylinus*'s frequency response shows little variation despite the varying incubation times. This is beneficial as the bacterial cellulose synthesis study features bacterial cells exposed to an electrical field for 14 days. Due to little change in their frequency response while exposed to an electric field for long periods of time, this indicates that the cell's composition may have minimal compositional changes.

5.3 Bacterial Cellulose Synthesis Under an Electric Field Results at 1 V_{pp}, 2 V_{pp}, and 5 V_{pp}

This section of results features the bacterial cellulose synthesis study at polarization voltages of 1 V_{pp}, 2 V_{pp}, and 5 V_{pp}. Each experiment was repeated three times for each polarization voltage featuring magnitudes of electric fields ranging from 10 – 100 kV/m.

Figure 18 represents the complete analysis one of the experimental studies (5V, Experiment 1) by showing the fluorescent and brightfield percent change in intensity (T-T_0) versus time (across 14 days) in all the regions. Each line on the plot is representative of each region (Region 1, 2, 3, 4, 5, 6, 4A).

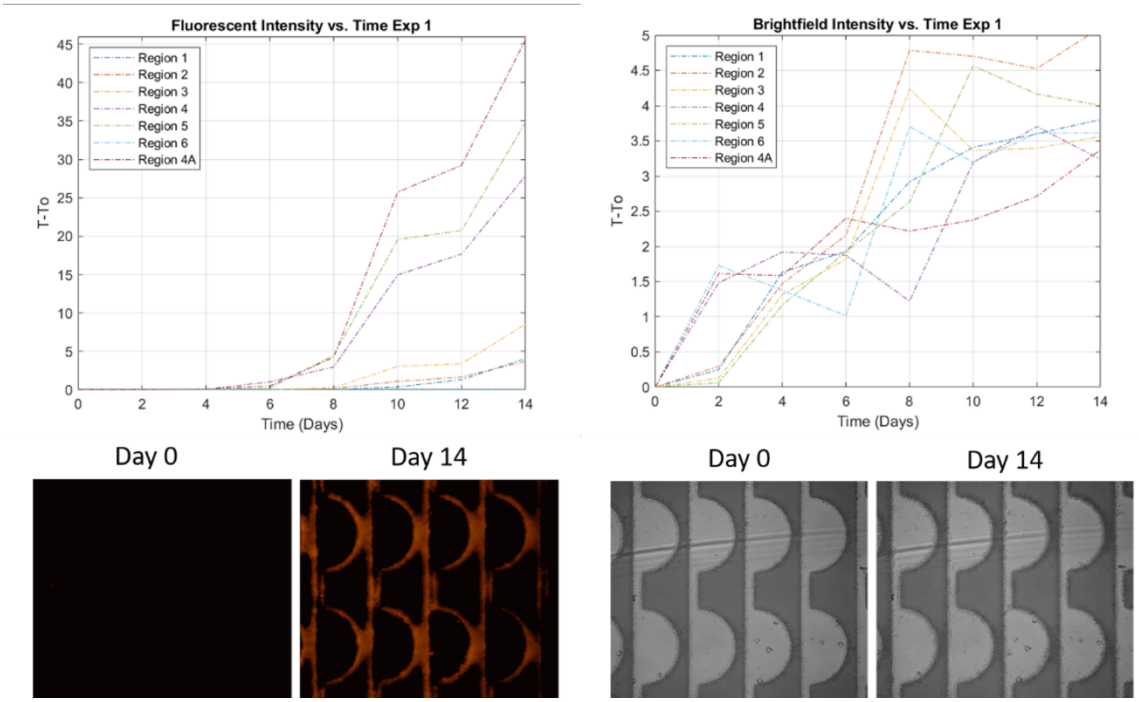

Figure 18: Complete Analysis of Experiment 1 at 5 V_{pp} for All Regions for the Fluorescent and Brightfield Change in Intensity

As expected, Region 4A represents the greatest change in fluorescent intensity for BC synthesis due to the highest electric field. The percent change in fluorescent intensity was followed up by Regions 4, 5, and 3, respectively in the following order. The percent change in fluorescent intensity for Region 1 and 2 behaved very similarly with each other and showed the least amount of fluorescence. Region 6 was analyzed to account for any free-floating cells that may synthesis BC since the simulation results showed an electric field potential. However, Region 6 showed little to no change in fluorescent intensity. As for the brightfield images, the trends behaved very erratically for Regions 1, 2, 3, 4, 5, and 6, except for Region 4A still showing the greatest change in intensity and highest enrichment region.

The rest of the experiments followed a very similar trend (2 V_{pp} and 5 V_{pp}). However, 1 V_{pp} did not follow this trend. This could be due to the very weak electric field not trapping enough bacterial cells or stimulating BC synthesis. Thus, not prompting enough of a percent change in fluorescent intensity at that the polarization voltage of 1 V_{pp}.

The rest of the results will specially feature Region 4A for each polarization voltage. Figures 19 – 24 highlights the percent change in fluorescent and brightfield intensity for each polarization voltage for Regions 4A by showing where *K. xylinus* is most concentrated due to the highest electric field gradient.

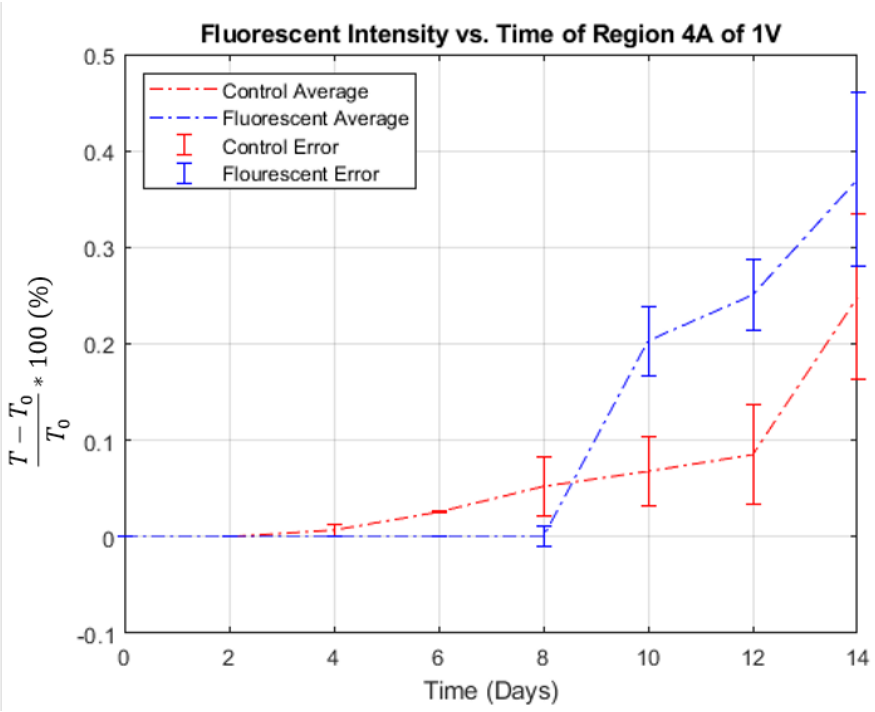

Figure 19: Plot of the Fluorescent Intensity versus Control Intensity and their standard deviations for Region 4A at 1 V_{pp}. This data represents the average of 8 Ti-microelectrodes per experiment (24 Ti-microelectrodes total) for the Fluorescent data and the Control data.

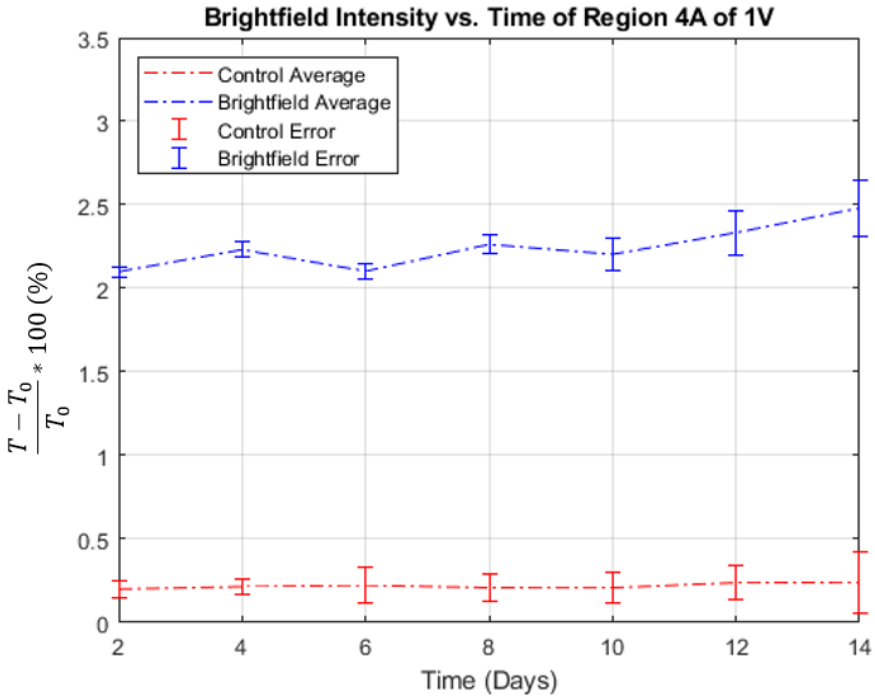

Figure 20: Plot of the Brightfield Intensity versus Control Intensity and their standard deviations for Region 4A at 1 Vpp. This data represents the average of 8 Ti-microelectrodes per experiment (24 Ti-microelectrodes total) for the Brightfield data and the Control data.

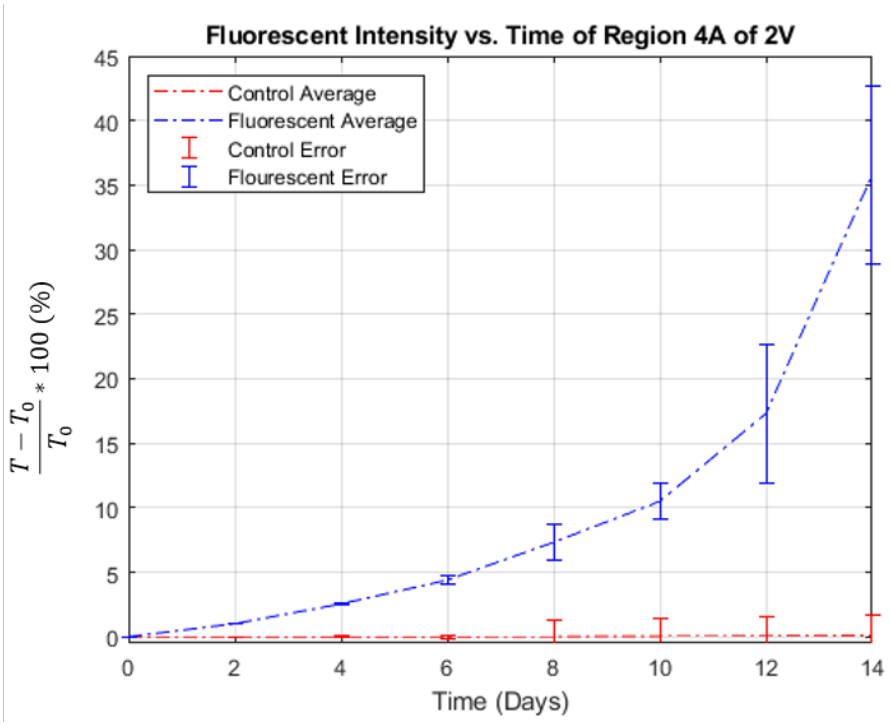

Figure 21: Plot of the Fluorescent Intensity versus Control Intensity and their standard deviations for Region 4A at 2 V_{pp}. This data represents the average of 8 Ti-microelectrodes per experiment (24 Ti-microelectrodes total) for the Fluorescent data and the Control data.

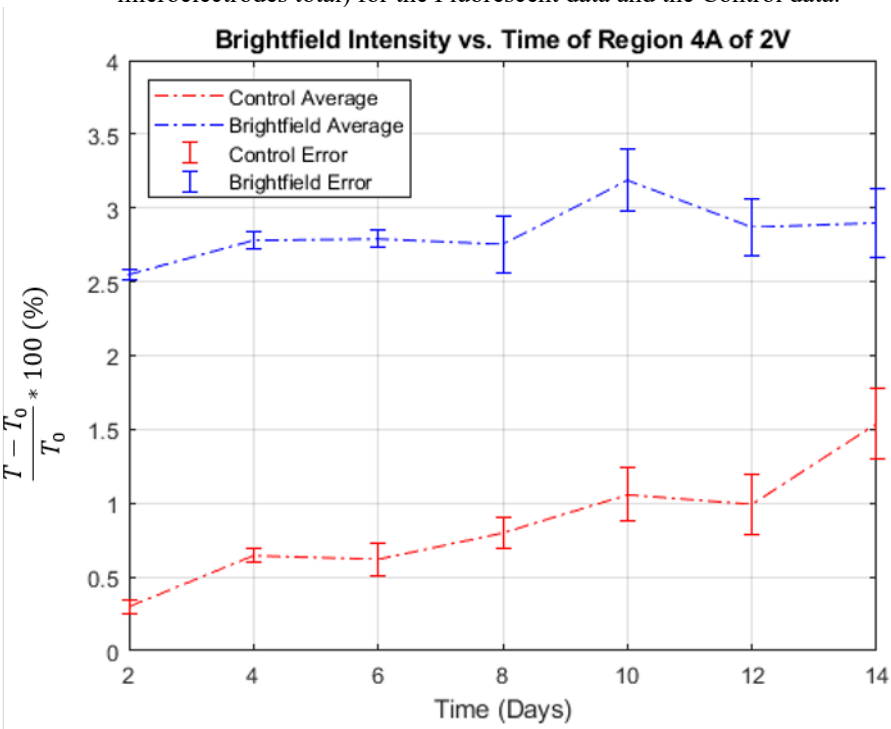

Figure 22: Plot of the Brightfield Intensity versus Control Intensity and their standard deviations for Region 4A at 2 V_{pp}. This data represents the average of 8 Ti-microelectrodes per experiment (24 Ti-microelectrodes total) for the Brightfield data and the Control data.

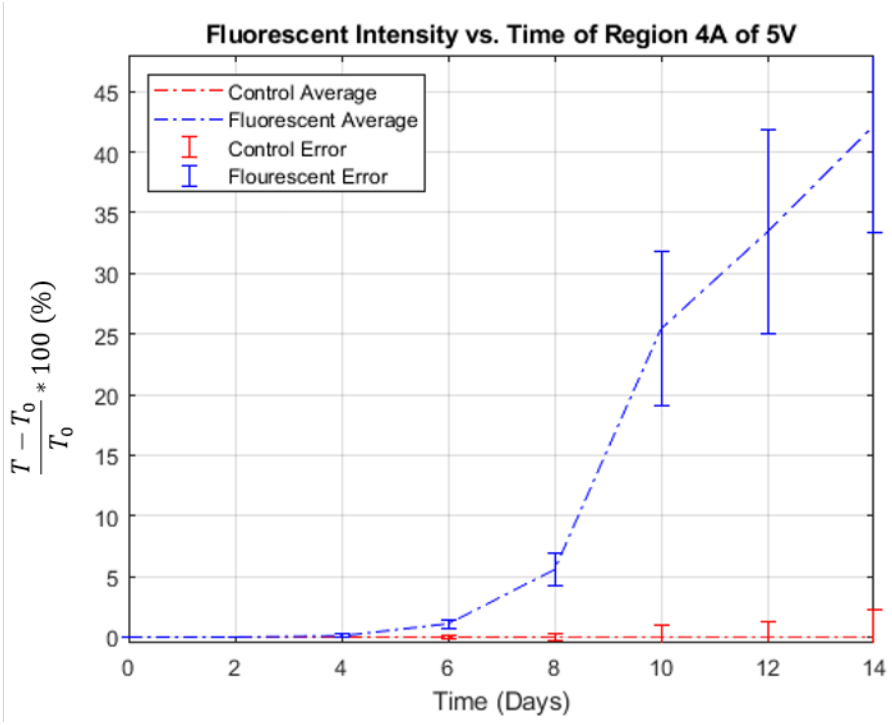

Figure 23: Plot of the Fluorescent Intensity versus Control Intensity and their standard deviations for Region 4A at 5 V_{pp}. This data represents the average of 8 Ti-microelectrodes per experiment (24 Ti-microelectrodes total) for the Fluorescent data and the Control data.

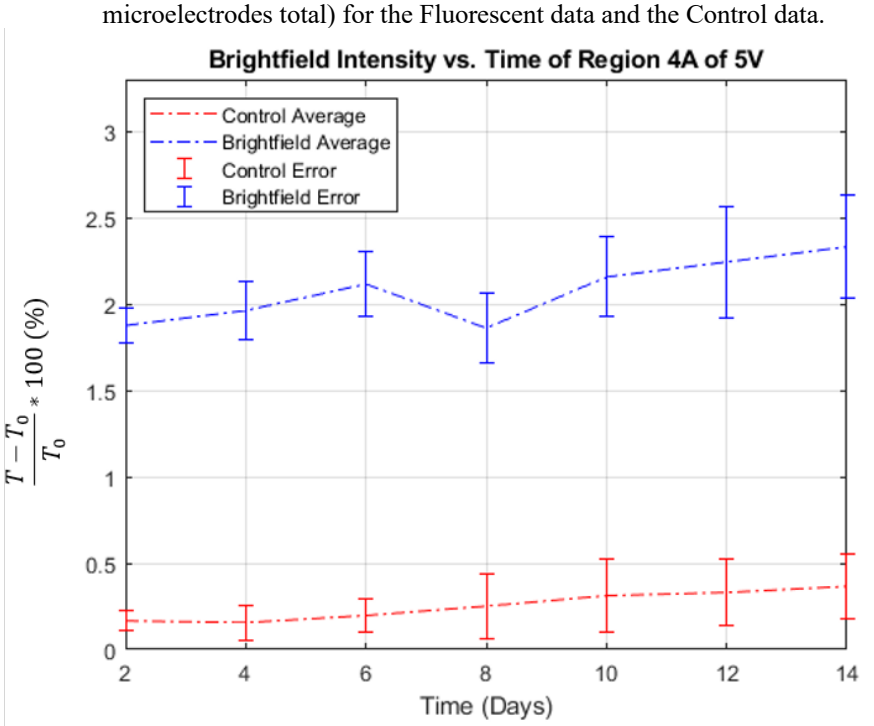

Figure 24: Plot of the Brightfield Intensity versus Control Intensity and their standard deviations for Region 4A at 5 V_{pp}. This data represents the average of 8 Ti-microelectrodes per experiment (24 Ti-microelectrodes total) for the Brightfield data and the Control data.

As mentioned, Region 4A shows the highest percent change than any other region across all experiments for the fluorescent intensity and the brightfield intensity. Details for Regions 1, 2, 3, 4, and 6 are not represented, as they are not regions of interest as determined by the ANSYS results since those regions have weaker electric fields. Appendix B highlights details of Regions 4A and Region 5 for each individual experiment.

Table 5 and 6 summarizes the fluorescent and brightfield change in intensity for Region 4A results at Day 14 along with the respective magnitudes of electric field.

Table 5: Summary of the Fluorescent and Control Change in Intensity for Region 4A at Day 14

	Fluorescent (%)	**Control (%)**
1 V: 11.6 kV/m	0.370	0.248
2 V: 21.5 kV/m	35.683	0.099
5 V: 54 kV/m	42.165	0.038

Table 6: Summary of the Brightfield and Control Change in Intensity for Region 4A at Day 14

	Brightfield (%)	**Control (%)**
1 V	2.240	2.898
2 V	1.359	2.480
5 V	1.965	2.331

The controls were analyzed the same way as a comparison to the data. The control experiments were run very similarly over the 14 days, however, with the electric field turned off. This was to observe the potential of electric fields and if they have capabilities to promote BC synthesis. By having controls, we can observe BC synthesis under normal

conditions in a microfluidic reactor. While the control experiments show some fluorescence, it is significantly less than other regions within the electric field potential.

Figure 25 and 26 shows the difference in the experimental average intensity for Region 4A of all 8 data points (each semicircular Ti-microelectrode) for each experiment for 1 V_{pp}, 2 V_{pp}, 5 V_{pp} for the fluorescent and brightfield experiments.

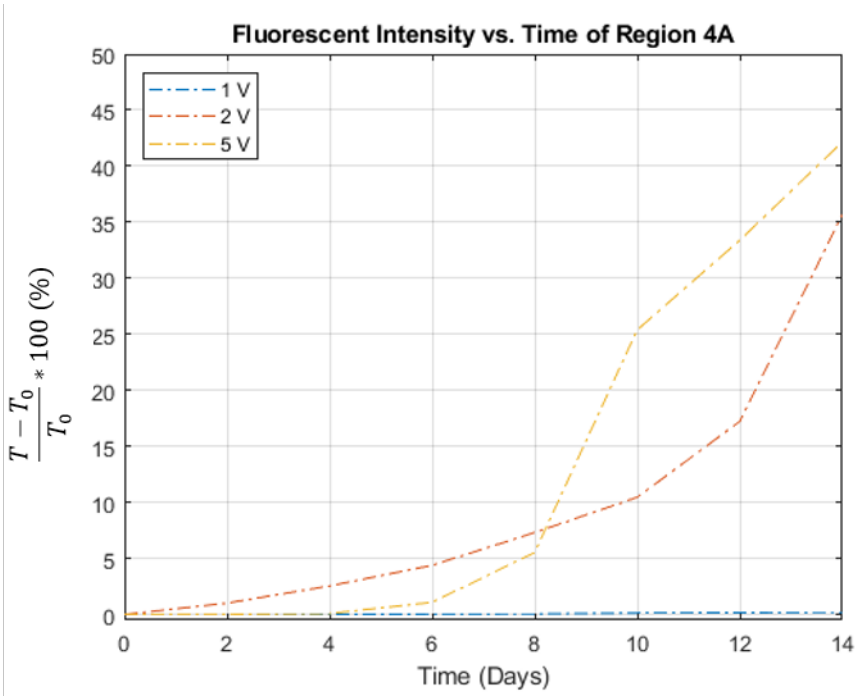

Figure 25: Plot of the Fluorescent Intensity for Region 4A at all voltages (1 V_{pp}, 2 V_{pp}, and 5 V_{pp}). This data represents the difference of the Fluorescent data and the Control data to normalize the results. It can be seen that 5 V_{pp} shows the greatest Change in Intensity and 1 V_{pp} with the least Change in Intensity.

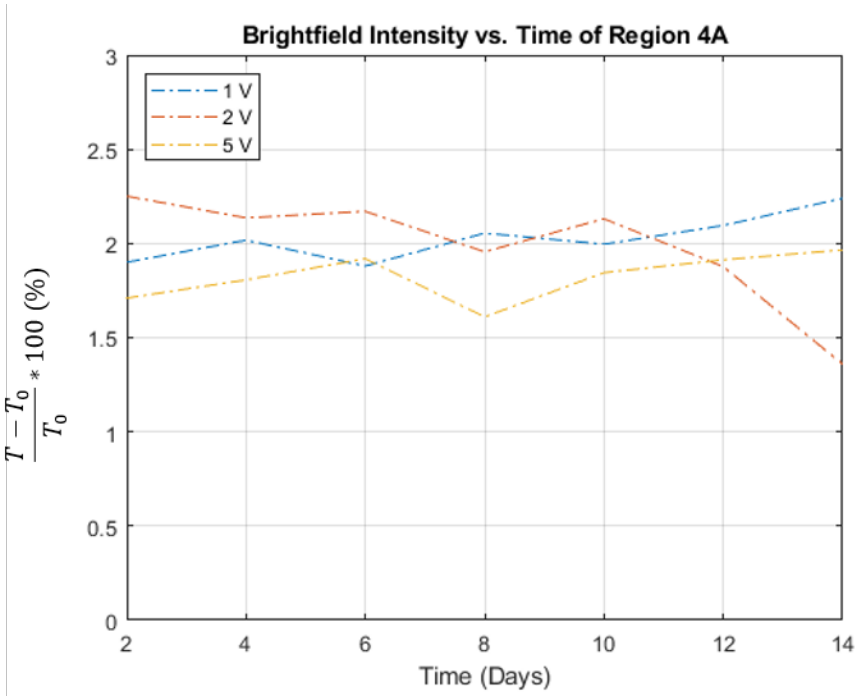

Figure 26: Plot of the Brightfield Intensity for Region 4A at all voltages (1 V_{pp}, 2 V_{pp}, and 5 V_{pp}). This data represents the difference of the Brightfield data and the Control data to normalize the results. It can be seen that the intensity slightly trends upward with the exception of 2 V_{pp}.

5.3.1 A Closer Look at 1 V_{pp} With Modified Results

Due to the very weak electric field at 1 V_{pp} and the minimal positive DEP response of *K. xylinus*, an experiment was done with a modified protocol to see if this is due to the lack of cells or electric field present. Therefore, 50-100 µL of the experimental sample was injected into the microfluidic chamber. Then, then sample was given time to stabilize for about 30 minutes at 5 V_{pp} at 750 kHz. After *K. xylinus* stabilized, the polarization voltage was changed to 1 V_{pp}. This was to ensure that as many cells could trap at the leading edges of the microelectrode in order to observe how the bacterial cells would behave while under the electric field after changing the polarization voltage. Figure 27 highlights the results of the experiment, which shows very similar trends to the original 1 V_{pp} experiment.

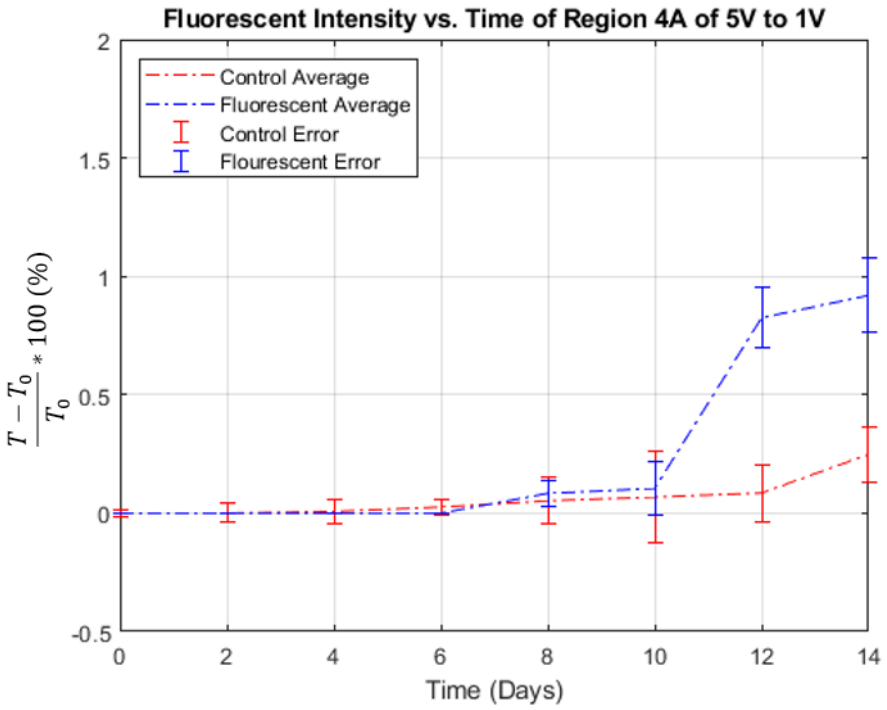

Figure 27: Plot of the Fluorescent Intensity versus Control Intensity and their standard deviations for Region 4A at 5 V_{pp} and then changed to 1 V_{pp} after the bacterial cells stabilized. This data represents the average of 8 Ti-microelectrodes per experiment (24 Ti-microelectrodes total) for the Fluorescent data and the Control data.

There was a very similar DEP response and change in fluorescent intensity compared to the original 1 V_{pp} study. The new fluorescent change in intensity value for this study was roughly 0.920 % compared to the original 0.370 %. This shows that despite the number of bacterial cells present, the magnitude of electric field was the same, which indicates that the magnitude of electric field can potentially stimulate bacterial cellulose synthesis.

5.3.2 Region 5 Results of Bacterial Cellulose Synthesis

After analyzing all regions of interest (Region 1, 2, 3, 4, 4A, 5, and 6), Region 5 appeared to show a notable amount of fluorescence as well despite showing the lack of electric field distribution in that region at all polarization voltages (1 V_{pp}, 2 V_{pp}, 5 V_{pp},

and 7 V_{pp}). Therefore, a cross-sectional simulation of the Ti-microelectrodes was analyzed to observe how the electric field behaves.

Figure 28 shows the distribution of the magnitude and the electric field gradient at a polarization voltage of 5 V_{pp}. Due to the 350 nm height of the Ti-microelectrodes, this created the necessary electric field distribution to trap *K. xylinus* at the leading edges of the Ti-microelectrodes.

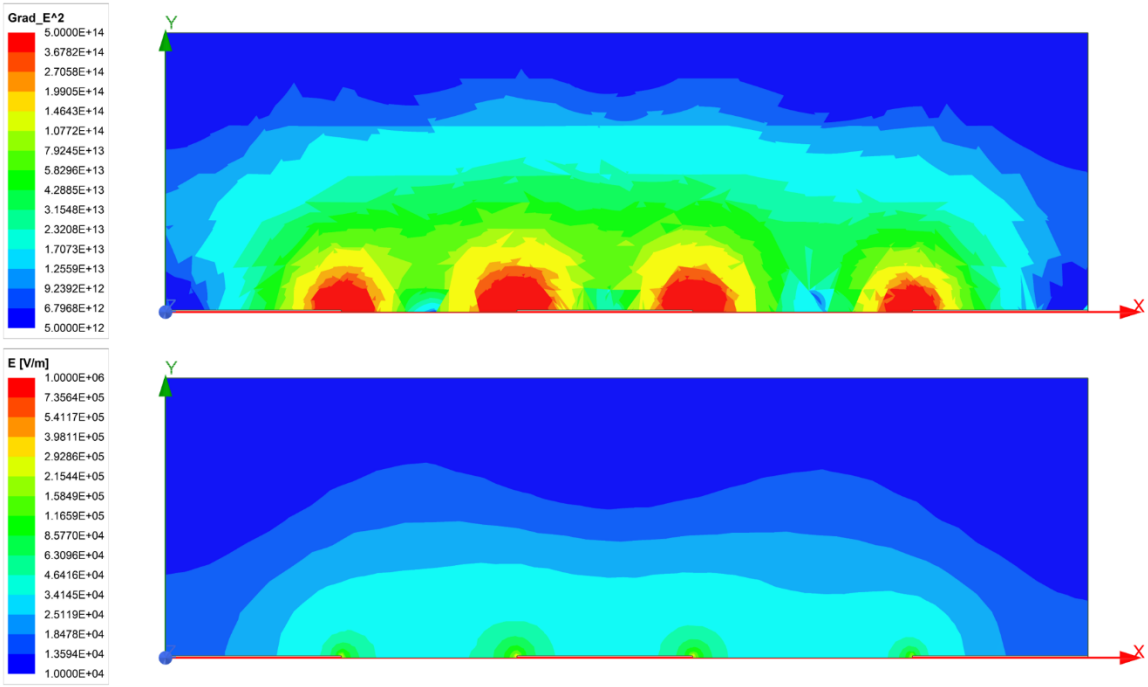

Figure 28: Cross-sectional Modeling of the Electric Field for the 350 nm high Ti-microelectrodes at 5 V_{pp} to further analyze Region 5. The modeled media around the electrodes was water with an electrical conductivity of 504 µS/cm. The simulations show that the magnitude of the electric field is directly. By keeping the magnitude less than 10^5 V/m, this ensures optimal cell viability of *K. xylinus* and prevents electrical lysis.

Due to the height of the electrode and these simulation results, this could indicate why there is a significant amount of BC synthesis at Region 5. While Region 5 was not a region of interest based off the initial modeling results, this shows that this magnitude of

electric field can potentially promote BC synthesis. Due to this, Region 5 shows the second greatest percent change in fluorescent intensity.

Figure 29 shows the percent difference in the experimental average intensity for Region 5 of all 8 data points (each semicircular Ti-microelectrode) for each polarization voltage at 1 V_{pp}, 2 V_{pp}, and 5 V_{pp}.

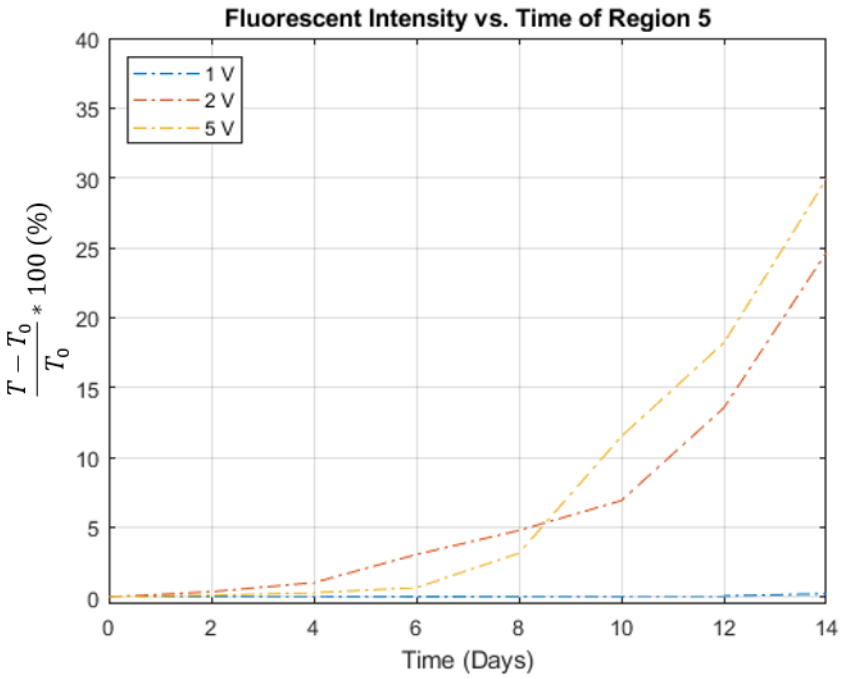

Figure 29: Plot of the Fluorescent Intensity for Region 5 at all voltages (1 V_{pp}, 2 V_{pp}, and 5 V_{pp}). This data represents the difference of the Fluorescent data and the Control data to normalize the results. It can be seen that 5 V_{pp} shows the greatest Change in Intensity and 1 V_{pp} with the least Change in Intensity.

5.4 Discussion

Based on these extensive studies and results, I am able to show that it is possible to stimulate BC synthesis by using DEP techniques to induce an electric field in a microfluidic reactor. There are a number of possibilties and theories as to why this can

occur. Possible experiments that can help address what specifically is happening to *K. xylinus* while under and eleectric field will be addressed in future work.

Some possibilties that can explain why electric fields promote BC synthesis could be due to the biological composition and its metabolic pathways of *K. xylinus*. For example, the presence of hydrogen is beneficial to cell growth due to the bonds necessary for BC, but can be limited without the presence of oxygen which is necessary for the *K. xylinus* to undergo its metabolic growth cycle. However, while the bacterial cells are under the influence of an electric field, the electrolysis of water could create enough oxygen in the solution in the microfluidic chamber for these metabolic pathways. This is because the presence of hydrogen is beneficial to cell growth due to the bonds necessary for BC but can be limited without the presence of oxygen. This could be the reason why the bacterial cells are able to continue synthesizing BC over a long period of time (14 days). However, it is unclear if this the reason why as further experiments need to be done to see how this experimental set up affects the metabolic pathways of *K. xylinus*.

Another potential reason could be due to the electrical phenomenon of cell electroporation in microfluidics. As mentioned previously, this is an important phenomenon as the magnitude of the electric field can dictate how materials can move in and/or out of a cell via the cell wall. While *K. xylinus* is suspended in the media, there is a natural distribution of charges. When an electric field is introduced, this redistributes the charges and creates the transmembrane potential necessary to generate pores along the membrane to facilitate materials moving in and/or out of the cell. This technique could be facilitating materials necessary for BC synthesis into the bacterial cell quicker than

traditional metabolic processes or extruding cellulose fibers outside the cell at an accelerated rate. Electroporation in microfluidics can introduce this phenomenon at magnitudes as little as 15 kV/m (but are not limited to this number), and the BC synthesis study features magnitudes ranging from 10 – 100 kV/m. This means that electroporation could potentially influence the synthesis of BC by *K. xylinus* [14].

Figure 23 indicates that at 5 V_{pp}, the percent change in fluorescent intensity starts to slow down after Day 10. The exponential growth occurs between day 8 – 10 at 5 V_{pp} versus the exponential increase over the 14-day period for the 2 V_{pp} for Region 4A. This could indicate the possibility of BC synthesis coming to a stop due to long term exposure of the electric field. This could be due to the lack of necessary functional groups and materials necessary for BC synthesis. Studies have shown that long-term exposure to an electric field can halt the BC synthesis process after a long period of time [19, 24]. However, these results indicate that *K. xylinus* can continue synthesizing BC until Day 14. This could be due to *K. xylinus* responding and adapting to the electric field over time. Bacterial cells respond to changes in their environment and adapt to survive, which could be why early on, BC needs a couple days to start synthesizing BC while in the microfluidic reactor. Once the threshold is reached, this could be why the process slows down due to a lack of materials necessary for cell survival and functional groups necessary for the BC bonds.

CHAPTER SIX

CONCLUSIONS AND FUTURE WORK

6.1 Conclusion

These studies demonstrate that *K. xylinus* has a positive DEP response from 0.25 – 1 MHz and behave similarly despite varying culture ages of 24, 48, and 96 hours. *K. xylinus* can synthesize BC under different magnitudes (approximately 21.5 – 54 kV/m) of electric fields at polarization voltages of 2 V_{pp} and 5 V_{pp}. At 1 V_{pp}, the magnitude of the electric field (approximately 11.6 kV/m) was not strong enough to promote BC synthesis. This study has shown that these magnitudes of electric fields have to potential to promote BC synthesis. However, how this mechanism occurs is still unclear. To further understand how this occurs, more extensive studies need to be done on a molecular and biological level to see how to microorganism responds, which will be addressed in Section 6.2.

6.2 Future Work

Many of the biological processes and metabolic processes help give an understanding of how BC is synthesized in a static culture. However, there is limited information published on how the biological and metabolic processes are affected while under an electric field. In order to understand these processes, it would be beneficial to

understand how electric fields affect *K. xylinus* and its fiber composition visually. Our microscope is unable to visualize what is happening to the BC fiber itself and the cell wall. Experiments at the Clemson Light Imaging Facility (CLIF) has high-end confocal microscopes and SEM microscopes to better visualize what is happening to *K. xylinus* on a nanoscale. By doing so, we can narrow down the microorganism's changes. By doing so, this will help understand physical and/or metabolic changes while under an electric field. By understanding this, it will bring us one step closer to being able to understand and manipulate BC by using a DEP induced electric field to arbitrary locations.

REFERENCES

1. Gama, Miguel, Paul Gatenholm, and D Klemm. *Bacterial Nanocellulose: A Sophisticated Multifunctional Material*. Boca Raton, FL: CRC Press, 2013. Print.

2. Ross, P., Mayer, R., & Benziman, A. N. D. M. (1991). Cellulose biosynthesis and function in bacteria positive control. *Microbiological Reviews*, *55*(1), 35–58.

3. Esa, F., Tasirin, S. M., & Rahman, N. A. (2014). Overview of Bacterial Cellulose Production and Application. *Agriculture and Agricultural Science Procedia*, *2*, 113–119. https://doi.org/10.1016/j.aaspro.2014.11.017\

4. Yamada, Y., Yukphan, P., Vu, H. T. L., Muramatsu, Y., Ochaikul, D., Tanasupawat, S., & Nakagawa, Y. (2012). Description of Komagataeibacter gen. nov., with proposals of new combinations (Acetobacteraceae). *Journal of General and Applied Microbiology*, *58*(5), 397–404. https://doi.org/10.2323/jgam.58.397

5. A. Melnick L. Sheng, M. C. (2016). HHS Public Access. *Physiology & Behavior*, *176*(1), 100–106. https://doi.org/10.1016/j.coisb.2017.03.005.Mechanisms

6. Pethig, R.; Menachery, A.; Pells, S.; DeSousa, P. Dielectrophoresis: a review of applications for stem cell research. J. Biomed. Biotechnol. 2010, 2010, 1–7, doi:10.1155/2010/182581.

7. Costa, A. F. S., Almeida, F. C. G., Vinhas, G. M., & Sarubbo, L. A. (2017). Production of bacterial cellulose by Gluconacetobacter hansenii using corn steep liquor as nutrient sources. *Frontiers in Microbiology*, *8*(OCT), 1–12. https://doi.org/10.3389/fmicb.2017.02027

8. Wu, D., Li, X., Shen, C., Lu, J., Chen, J., and Xie, G. (2014). Decreased ethyl carbamate generation during Chinese rice wine fermentation by disruption of CAR1 in an industrial yeast strain. Int. J. Food Microbiol. 180, 19–23. doi: 10.1016/j.ijfoodmicro.2014.04.007

9. Sano, M. B., Rojas, A. D., Gatenholm, P., & Davalos, R. V. (2010). Electromagnetically controlled biological assembly of aligned bacterial cellulose nanofibers. *Annals of Biomedical Engineering*, *38*(8), 2475–2484. https://doi.org/10.1007/s10439-010-9999-0

10. Huang, Y., Holzel, R., Pethig, R., and Wang, X.-B., Differences in the AC electrodynamics of viable and non-viable yeast cells determined through

combined dielectrophoresis and electrorotation studies, Physics in Medicine and Biology 37 (7), 1499-1517, 1992.

11. Kelsey C. Martin Mhatre V. Ho, J.-A. L. (2012). NIH Public Access. *Bone*, *23*(1), 1–7. https://doi.org/10.1109/JPROC.2003.820535.Dielectrophoresis-Based

12. Saxena, I. M., & Brown, R. M. (2005). Cellulose biosynthesis: Current views and evolving concepts. *Annals of Botany*, *96*(1), 9–21. https://doi.org/10.1093/aob/mci155

13. Sano, M. B., Davalos, R. V., & Gatenholm, P. (2009). Dielectrophoretic microweaving: Biofabrication of aligned bacterial nanocellulose for regenerative medicine. *Proceedings of the ASME Summer Bioengineering Conference 2009, SBC2009*, *PART A*, 563–564. https://doi.org/10.1115/SBC2009-206787

14. Movahed, S., & Li, D. (2011). Microfluidics cell electroporation. In *Microfluidics and Nanofluidics* (Vol. 10, Issue 4). https://doi.org/10.1007/s10404-010-0716-y

15. Gallegos, A. M. A., Carrera, S. H., Parra, R., Keshavarz, T., & Iqbal, H. M. N. (2016). Bacterial cellulose: A sustainable source to develop value-added products - A review. *BioResources*, *11*(2), 5641–5655. https://doi.org/10.15376/biores.11.2.Gallegos

16. Mattar, J. R., Turk, M. F., Nonus, M., Lebovka, N. I., El Zakhem, H., & Vorobiev, E. (2014). Electro-stimulation of *S. cerevisiae* wine yeasts by pulsed electric field and its effects on fermentation capacity. *Food and Bioprocess Technology*, *7*(11), 3328–3335. https://www.researchgate.net/publication/266398720_Stimulation_of_Saccharomyces_cerevisiae_Cultures_by_Pulsed_Electric_Fields

17. Hülsheger, H. et al. “Electric field effects on bacteria and yeast cells.” *Radiation and Environmental Biophysics* 22 (1983): 149-162.

18. Singhsa, P., Narain, R., & Manuspiya, H. (2018). Physical structure variations of bacterial cellulose produced by different Komagataeibacter xylinus strains and carbon sources in static and agitated conditions. *Cellulose*, *25*(3), 1571–1581. https://doi.org/10.1007/s10570-018-1699-1

19. Liu, M., Zhong, C., Zhang, Y. M., Xu, Z. M., & Qiao, C. S. (2016). Metabolic Investigation in Gluconacetobacter xylinus and Its Bacterial Cellulose Production under a Direct Current Electric Field. *Frontiers in Microbiology*, *7*(March), 1–12. https://doi.org/10.3389/fmicb.2016.00331

20. Esteban-Ferrer, D., Edwards, M. A., Fumagalli, L., Juárez, A., & Gomila, G. (2014). Electric polarization properties of single bacteria measured with

electrostatic force microscopy. *ACS Nano*, *8*(10), 9843–9849. https://doi.org/10.1021/nn5041476

21. Becker, F. F., Wang, X. B., Huang, Y., Pethig, R., Vykoukal, J., and Gascoyne, P. R. C., The removal of human leukaemia cells from blood using interdigitated microelectrodes, Journal of Applied Physics 27 , 2659-2662, 1994.
22. Andriani, D., Apriyana, A. Y., & Karina, M. (2020). The optimization of bacterial cellulose production and its applications: a review. *Cellulose*, *27*(12), 6747–6766. https://doi.org/10.1007/s10570-020-03273-9

23. Brown, R. M. Jr., Willison, J. H., and Richardson, C. L. (1976). Cellulose biosynthesis in Acetobacter xylinum: visualization of the site of synthesis and direct measurement of the in vivo process. Proc. Natl. Acad. Sci. U.S.A. 73, 4565–4569. doi: 10.1073/pnas.73.12.4565

24. Fijałkowski, K., Drozd, R., Zywicka, A., Junka, A. F., Kordas, M., & Rakoczy, R. (2017). Biochemical and cellular properties of Gluconacetobacter xylinus cultures exposed to different modes of rotating magnetic field. *Polish Journal of Chemical Technology*, *19*(2), 107–114. https://doi.org/10.1515/pjct-2017-0036

25. Liu, M., Zhong, C., Zheng, X., Ye, L., Wan, T., & Jia, S. R. (2017). Oriented bacterial cellulose-glass fiber nanocomposites with enhanced tensile strength through electric field. *Fibers and Polymers*, *18*(7), 1408–1412. https://doi.org/10.1007/s12221-017-1232-4

26. Baah-Dwomoh, A., Rolong, A., Gatenholm, P., & Davalos, R. V. (2015). The feasibility of using irreversible electroporation to introduce pores in bacterial cellulose scaffolds for tissue engineering. *Applied Microbiology and Biotechnology*, *Mc 0298*. https://doi.org/10.1007/s00253-015-6445-0

27. Fijałkowski, K., Żywicka, A., Drozd, R., Junka, A. F., Peitler, D., Kordas, M., Konopacki, M., Szymczyk, P., El Fray, M., & Rakoczy, R. (2016). Increased yield and selected properties of bacterial cellulose exposed to different modes of a rotating magnetic field. *Engineering in Life Sciences*, *16*(5), 483–493. https://doi.org/10.1002/elsc.201500151

28. Anderson, C. T., Carroll, A., Akhmetova, L., & Somerville, C. (2010). Real-time imaging of cellulose reorientation during cell wall expansion in Arabidopsis roots. *Plant Physiology*, *152*(2), 787–796. https://doi.org/10.1104/pp.109.150128

29. Thomas, J., Ingerfeld, M., Nair, H., Chauhan, S. S., & Collings, D. A. (2013). Pontamine fast scarlet 4B: A new fluorescent dye for visualising cell wall organisation in radiata pine tracheids. *Wood Science and Technology*, *47*(1), 59–75. https://doi.org/10.1007/s00226-012-0483-x

30. J, L., I, Z., & A, S. (2013). Super-resolution imaging with Pontamine Fast Scarlet 4BS enables direct visualization of cellulose orientation and cell connection architecture in onion epidermis cells. *BMC Plant Biology*, *13*, 226. http://linksource.ebsco.com/ls.941a0f3a-fc44-412f-81a4-365a06658f2f.false/linking.aspx?&sid=OVID:medline&id=pmid:24373117&id=doi:10.1186%2F1471-2229-13-226&issn=1471-2229&isbn=&volume=13&issue=1&spage=226&pages=226&date=2013&title=BMC+Plant+Biology&atitle

31. Thomas, J., Idris, N. A., & Collings, D. A. (2017). Pontamine fast scarlet 4B bifluorescence and measurements of cellulose microfibril angles. *Journal of Microscopy*, *268*(1), 13–27. https://doi.org/10.1111/jmi.12582

32. Mycologia, S., & Jun, N. M. (2017). *Two New Fluorescent Dyes Applicable for Visualization of Fungal Cell Walls* Author (s): H . C . Hoch , C . D . Galvani , D . H . Szarowski and J . N . Turner Stable URL : http://www.jstor.org/stable/3762339 Linked references are available on J. 97(3), 580–588.

33. Jacek, P., Dourado, F., Gama, M., & Bielecki, S. (2019). Molecular aspects of bacterial nanocellulose biosynthesis. *Microbial Biotechnology*, *12*(4), 633–649. https://doi.org/10.1111/1751-7915.13386

34. Pillet, F., Formosa-Dague, C., Baaziz, H., Dague, E., & Rols, M. P. (2016). Cell wall as a target for bacteria inactivation by pulsed electric fields. *Scientific Reports*, *6* (February), 1–8. https://doi.org/10.1038/srep19778

35. Sale, A. J. H., & Hamilton, W. A. (1967). BIOCHI1VflCA ET BIOPHYSICA ACTA 781 BBA 25 876 EFFECTS OF HIGH ELECTRIC FIELDS ON MICROORGANISMS I. KILLING OF BACTERIA AND YEASTS. *Biochim. Biophys. Acta*, *148*, 781–788.

36. Yang, L., Banada, P. P., Bhunia, A. K., & Bashir, R. (2008). Effects of Dielectrophoresis on growth, viability and immuno-reactivity of Listeria monocytogenes. *Journal of Biological Engineering*, *2*, 1–14. https://doi.org/10.1186/1754-1611-2-6

37. Lopez, M. C., Iglesias, F. J., Santamaria, C., & Dominguez, A. (1985). Dielectrophoretic behavior of yeast cells: Effect of growth sources and cell wall and a comparison with fungal spores. *Journal of Bacteriology*, *162*(2), 790–793. https://doi.org/10.1128/jb.162.2.790-793.1985

38. Fernandez, R. E., Rohani, A., Farmehini, V., & Swami, N. S. (2017). Review: Microbial analysis in dielectrophoretic microfluidic systems. *Analytica Chimica Acta*, *966*, 11–33. https://doi.org/10.1016/j.aca.2017.02.024

39. Zhang, Y., Parker, E. R., Rao, M. P., Aimi, M. F., Mezic, I., & MacDonald, N. C. (2004). Titanium bulk micromachining for biomems applications: A DEP device as a demonstration. *American Society of Mechanical Engineers, Micro-Electro Mechanical Systems Division, (Publications) MEMS*, *January 2015*, 45–48. https://doi.org/10.1115/IMECE2004-62136
40. Zhang, Y. T., Bottausci, F., Rao, M. P., Parker, E. R., Mezic, I., & MacDonald, N. C. (2008). Titanium-based dielectrophoresis devices for microfluidic applications. *Biomedical Microdevices*, *10*(4), 509–517. https://doi.org/10.1007/s10544-007-9159-y

41. Puttaswamy, S. V., Sivashankar, S., Chen, R. J., Chin, C. K., Chang, H. Y., & Liu, C. H. (2010). Enhanced cell viability and cell adhesion using low conductivity medium for negative dielectrophoretic cell patterning. *Biotechnology Journal*, *5*(10), 1005–1015. https://doi.org/10.1002/biot.201000194

42. Keck D, Stuart C, Duncan J, Gullette E, Martinez-Duarte R. Highly Localized Enrichment of Trypanosoma brucei Parasites Using Dielectrophoresis. Micromachines (Basel). 2020 Jun 26;11(6):625. doi: 10.3390/mi11060625. PMID: 32604888; PMCID: PMC7344920.

43. Rosenthal, A., & Voldman, J. (2005). Dielectrophoretic traps for single-particle patterning. *Biophysical Journal*, *88*(3), 2193–2205.

44. Islam M, Keck D, Gilmore J, Martinez-Duarte R. Characterization of the Dielectrophoretic Response of Different Candida Strains Using 3D Carbon Microelectrodes. Micromachines (Basel). 2020 Feb 28;11(3):255. doi: 10.3390/mi11030255. PMID: 32121163; PMCID: PMC7143313.

APPENDICES

Appendix A

Oxalic Acid Etch Rates For ITO-Microelectrode Devices

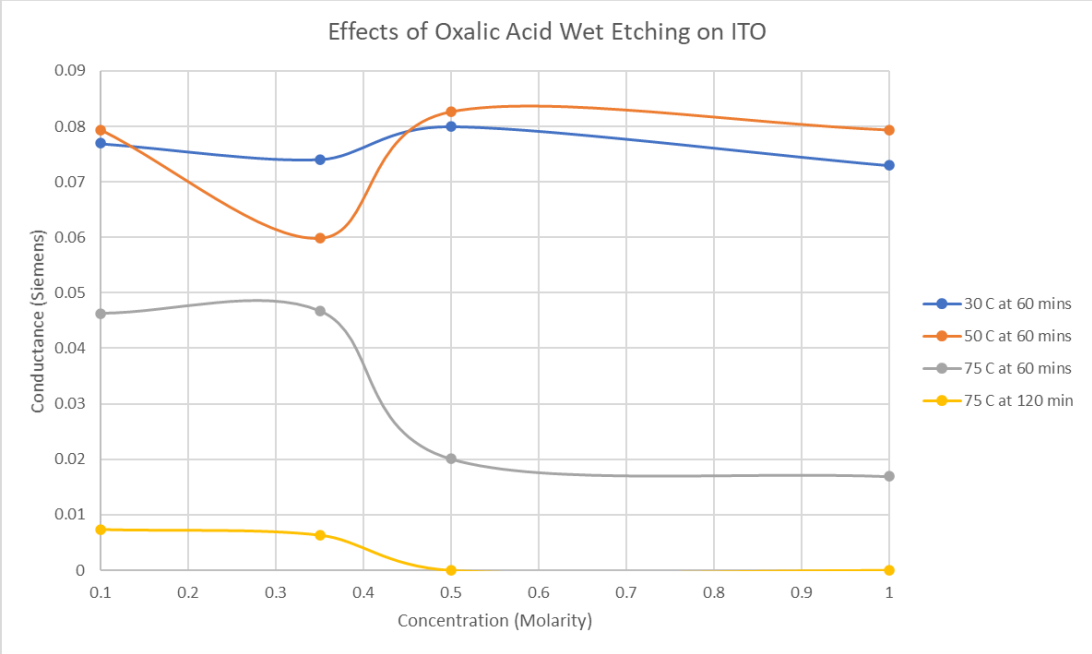

Figure A - 1: Conductance vs. Concentration of Oxalic Acid

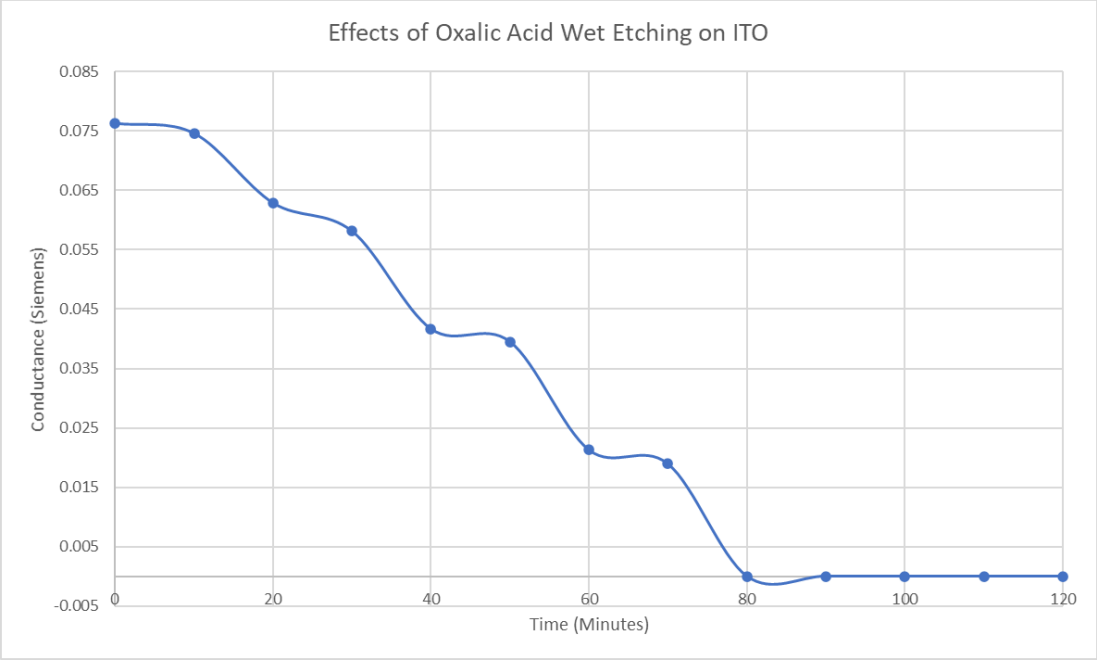

Figure A - 2: Conductance vs. 0.5 M Oxalic Acid over 120 mins

Appendix B

Fluorescent and Brightfield Plots for Region 4A and Region 5

All Florescent plots for Region 4A

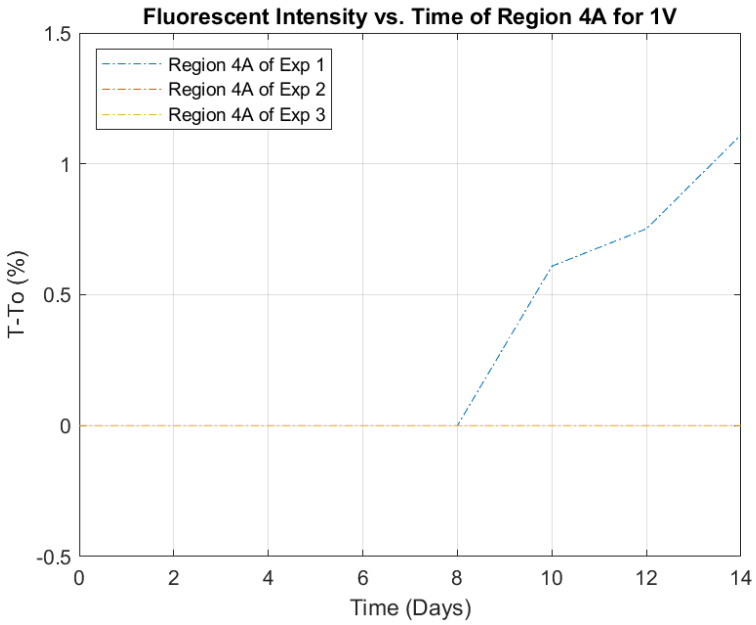

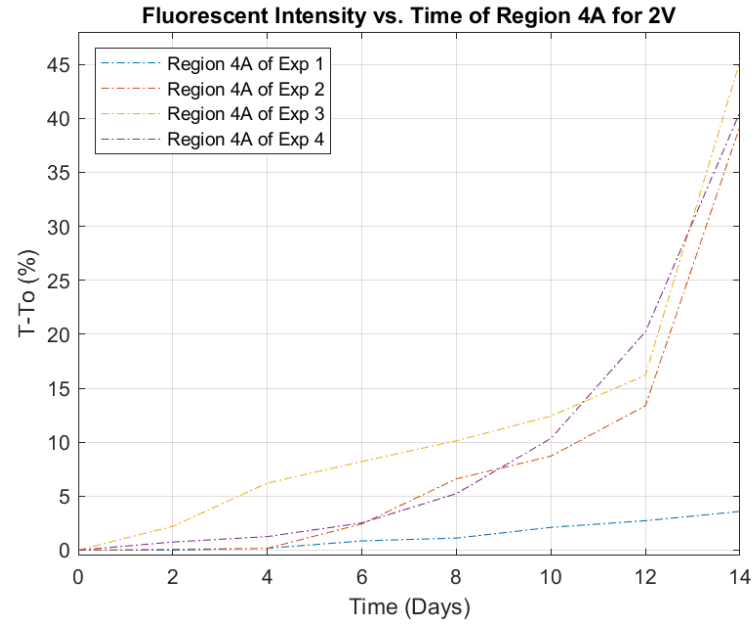

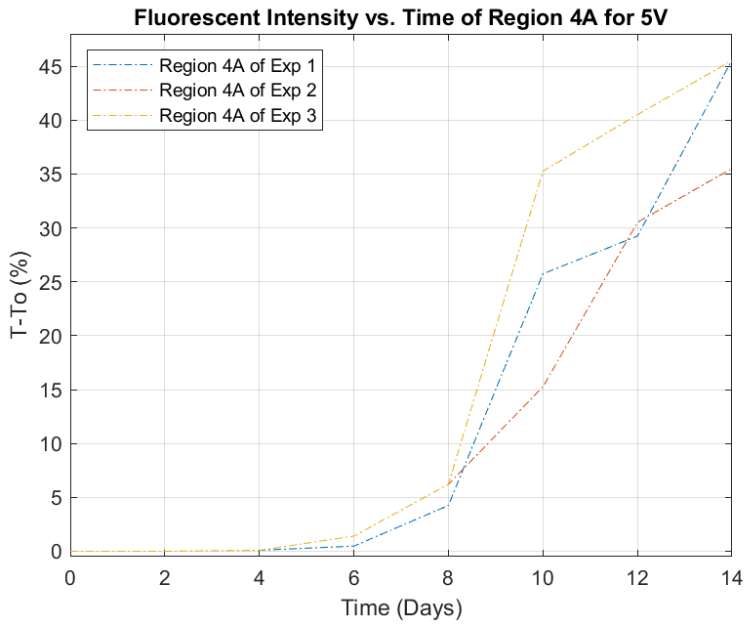

All Fluorescent plots for Region 5

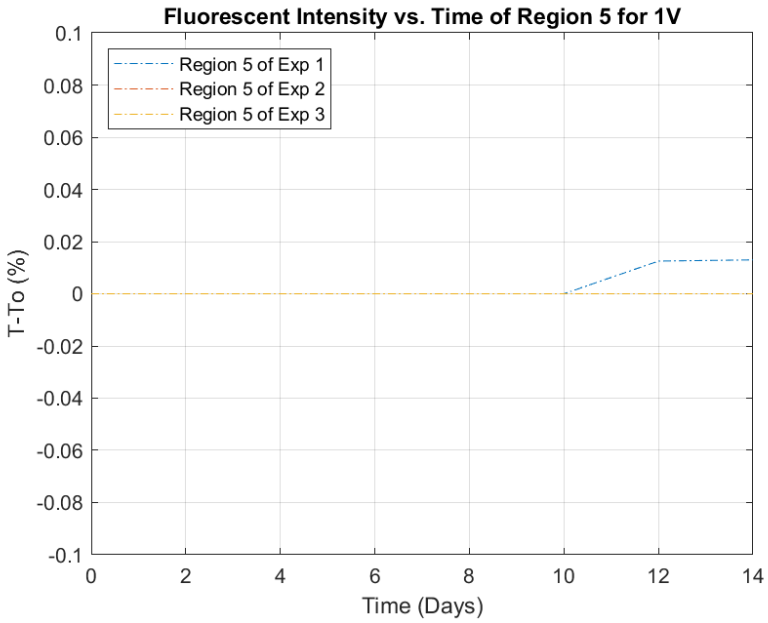

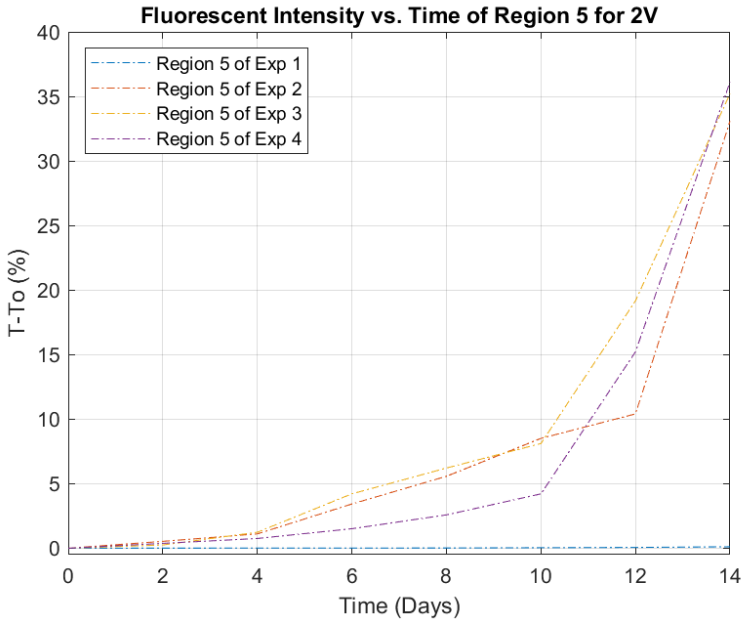

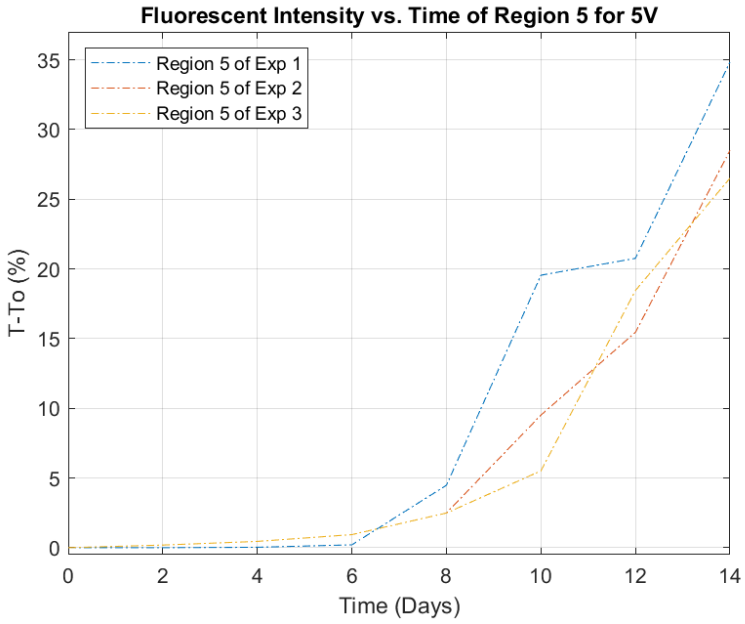

All Florescent Controls for Region 4A

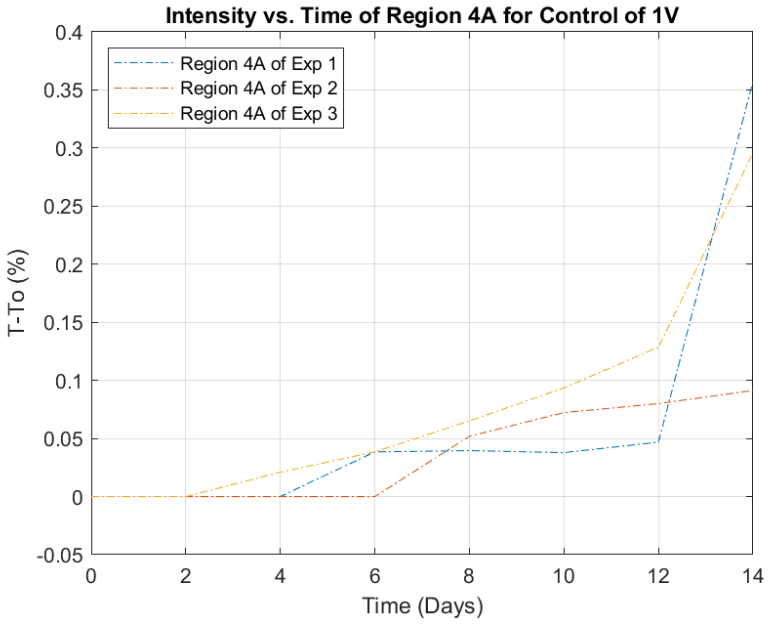
Intensity vs. Time of Region 4A for Control of 1V
Region 4A of Exp 1
Region 4A of Exp 2
Region 4A of Exp 3
T-To (%)
Time (Days)
0.4
0.35
0.3
0.25
0.2
0.15
0.1
0.05
0
-0.05
0
2
4
6
8
10
12
14

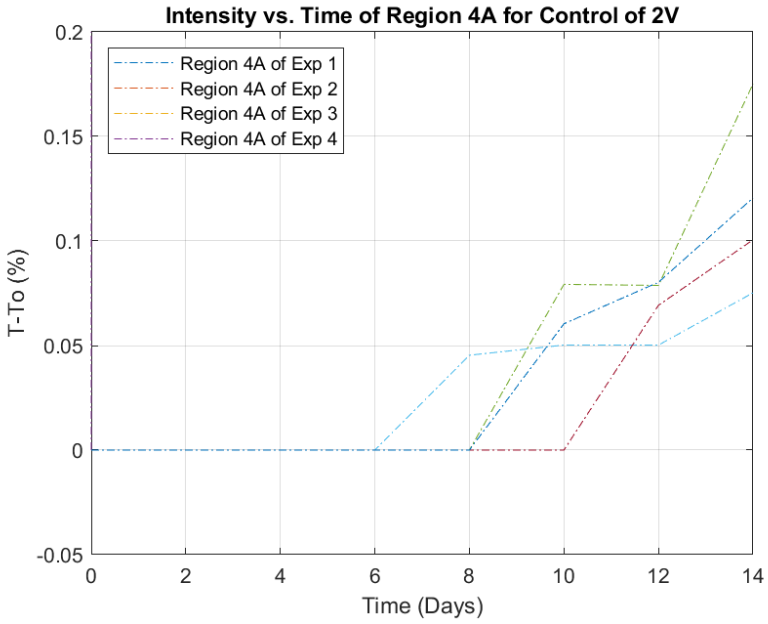
Intensity vs. Time of Region 4A for Control of 2V
Region 4A of Exp 1
Region 4A of Exp 2
Region 4A of Exp 3
Region 4A of Exp 4
T-To (%)
Time (Days)
0.2
0.15
0.1
0.05
0
-0.05
0
2
4
6
8
10
12
14

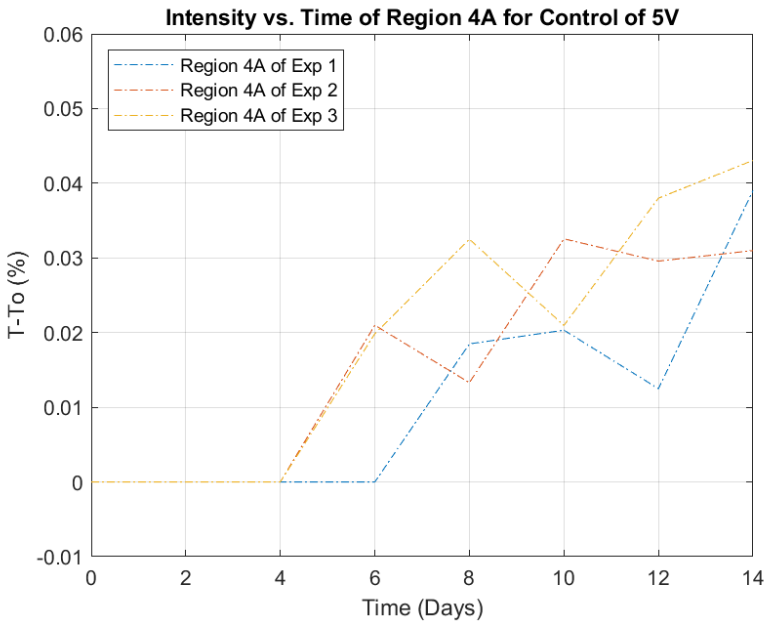

All Brightfield plots for Region 4A

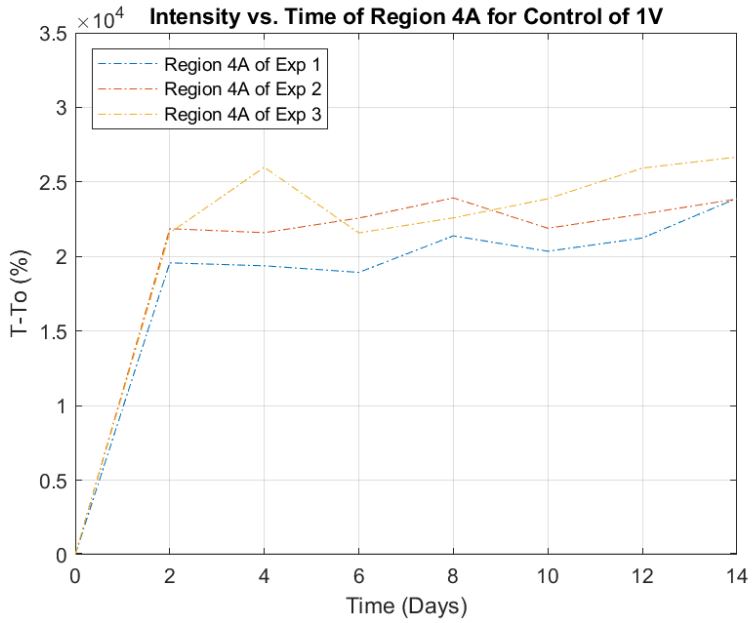

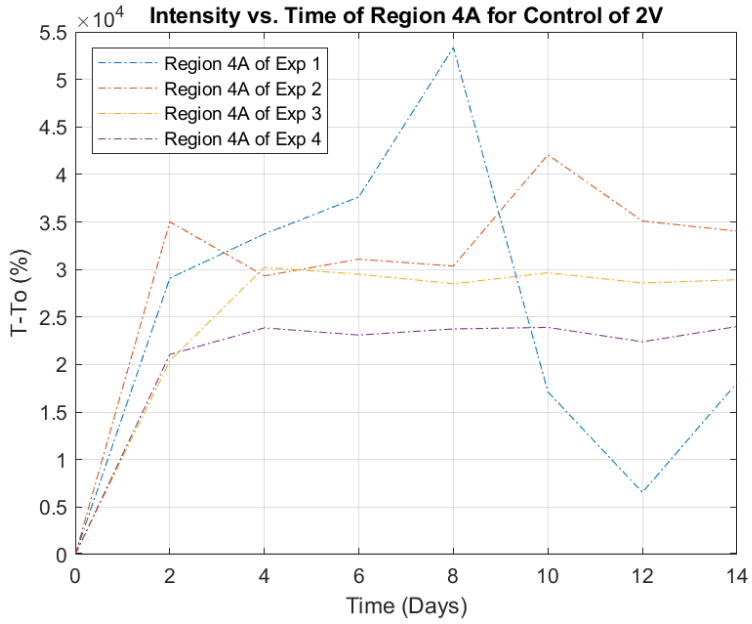

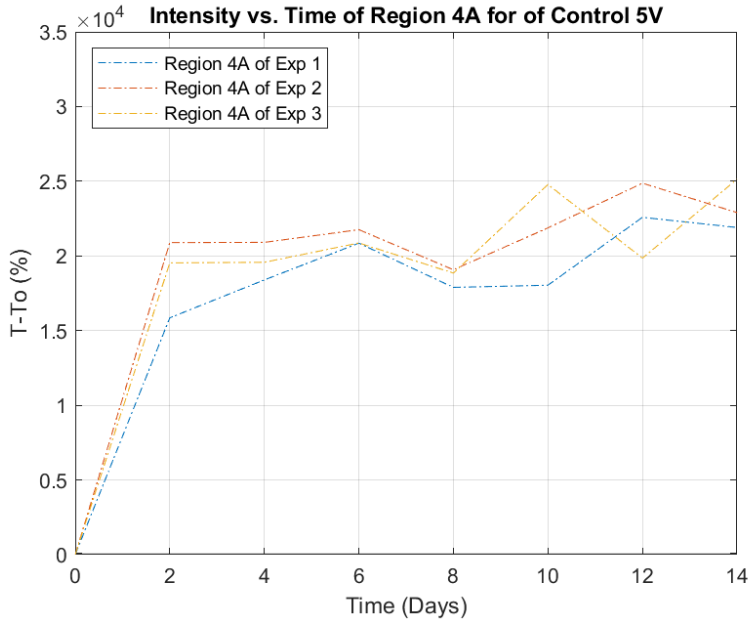

All Brightfield Plots for Region 5

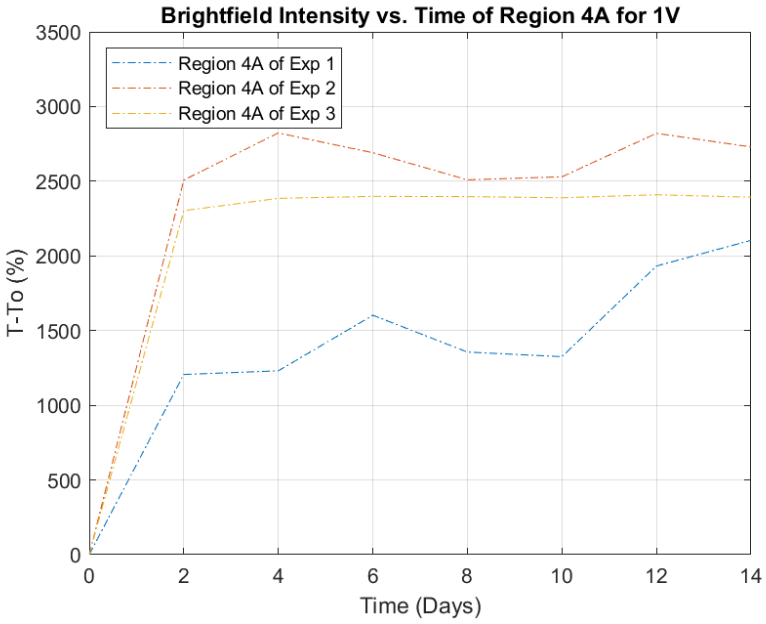
Brightfield Intensity vs. Time of Region 4A for 1V
Region 4A of Exp 1
Region 4A of Exp 2
Region 4A of Exp 3
T-To (%)
Time (Days)
0
500
1000
1500
2000
2500
3000
3500
0
2
4
6
8
10
12
14

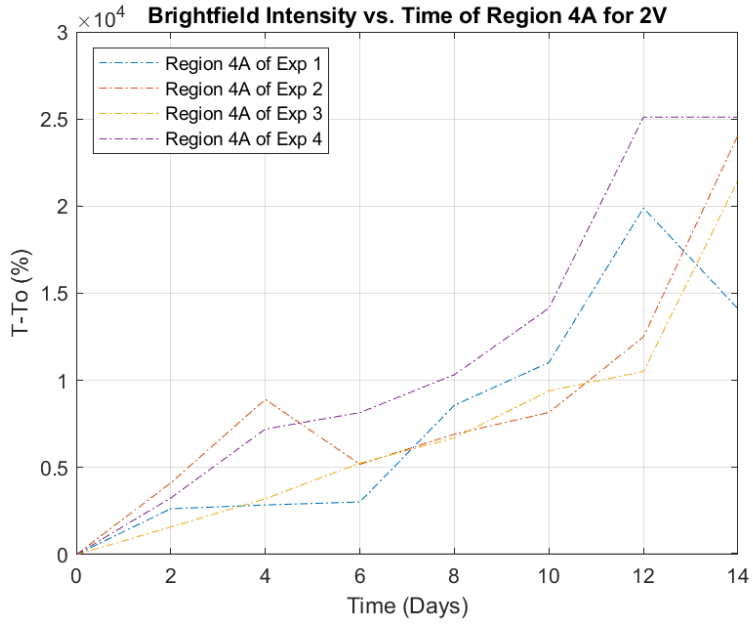
×10^4
Brightfield Intensity vs. Time of Region 4A for 2V
Region 4A of Exp 1
Region 4A of Exp 2
Region 4A of Exp 3
Region 4A of Exp 4
T-To (%)
Time (Days)
0
0.5
1
1.5
2
2.5
3
0
2
4
6
8
10
12
14

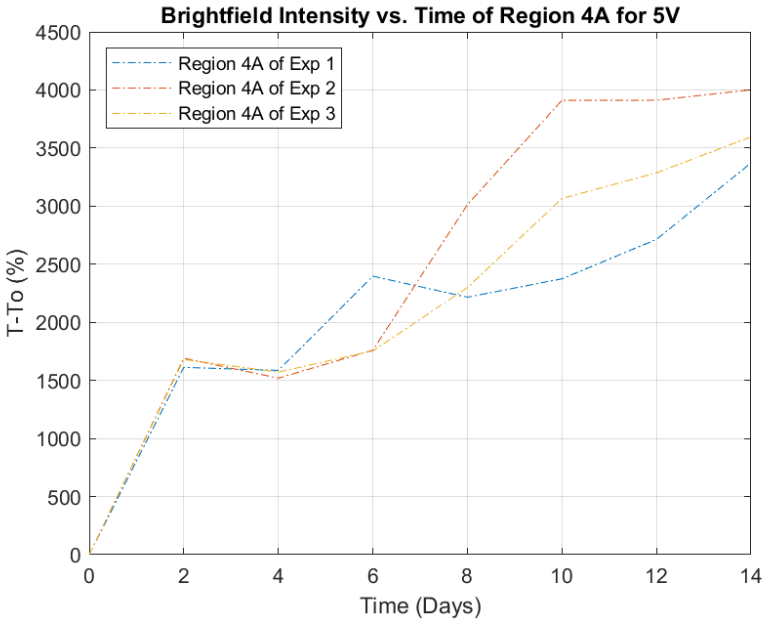
Brightfield Intensity vs. Time of Region 4A for 5V
Region 4A of Exp 1
Region 4A of Exp 2
Region 4A of Exp 3
T-To (%)
Time (Days)
0
500
1000
1500
2000
2500
3000
3500
4000
4500
0
2
4
6
8
10
12
14